

PVC: Progressive Visual Token Compression for Unified Image and Video Processing in Large Vision-Language Models

Chenyu Yang^{1,3*}, Xuan Dong^{1,3*}, Xizhou Zhu^{1,2*}, Weijie Su^{2*}, Jiahao Wang³, Hao Tian³, Zhe Chen^{2,4}, Wenhai Wang^{2,5}, Lewei Lu³, Jifeng Dai^{1,2}✉

¹Tsinghua University ²OpenGVLab, Shanghai AI Laboratory ³SenseTime Research
⁴Nanjing University ⁵The Chinese University of Hong Kong

{yangcy23, x-dong21}@mails.tsinghua.edu.cn, {zhuxizhou, daijifeng}@tsinghua.edu.cn,
suweijie@pjlab.org.cn, {wangjiahao2, tianhao2, luotto}@sensetime.com,
chenzhe98@smail.nju.edu.cn, whwang@ie.cuhk.edu.hk

Code: <https://github.com/OpenGVLab/PVC>

Abstract

Large Vision-Language Models (VLMs) have been extended to understand both images and videos. Visual token compression is leveraged to reduce the considerable token length of visual inputs. To meet the needs of different tasks, existing high-performance models usually process images and videos separately with different token compression strategies, limiting the capabilities of combining images and videos. To this end, we extend each image into a “static” video and introduce a unified token compression strategy called Progressive Visual Token Compression (PVC), where the tokens of each frame are progressively encoded and adaptively compressed to supplement the information not extracted from previous frames. Video tokens are efficiently compressed with exploiting the inherent temporal redundancy. Images are repeated as static videos, and the spatial details can be gradually supplemented in multiple frames. PVC unifies the token compressing of images and videos. With a limited number of tokens per frame (64 tokens by default), spatial details and temporal changes can still be preserved. Experiments show that our model achieves state-of-the-art performance across various video understanding benchmarks, including long video tasks and fine-grained short video tasks. Meanwhile, our unified token compression strategy incurs no performance loss on image benchmarks, particularly in detail-sensitive tasks.

1. Introduction

Recently, large Vision-Language Models (VLM) [2, 4, 18, 19, 59, 73, 74, 97, 98, 116, 117, 122] have achieved re-

*Equal contribution. This work is done when Chenyu Yang and Xuan Dong are interns at SenseTime Research. ✉Corresponding author: Jifeng Dai <daijifeng@tsinghua.edu.cn>.

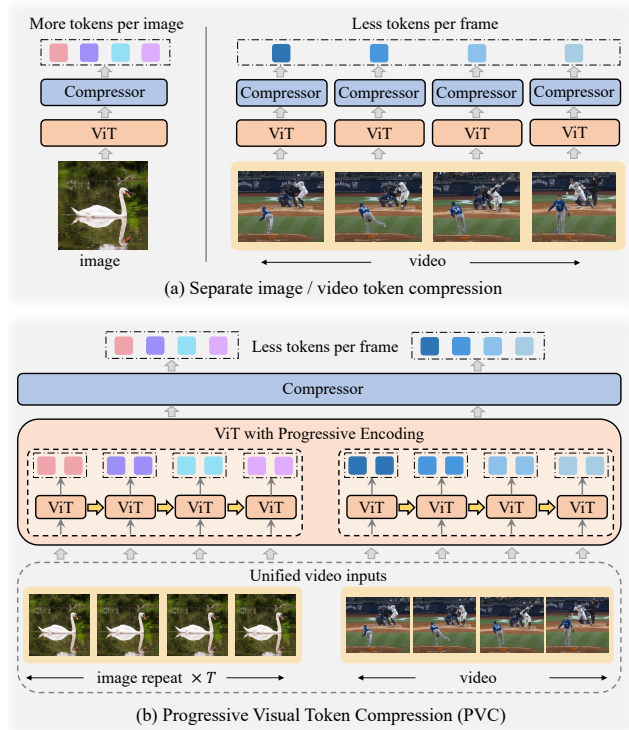


Figure 1. **Comparison of token encoding and compression in VLMs.** (a) Existing VLMs compress image and video tokens separately, leading to inconsistency: more tokens per image benefit image spatial perception, while videos tend to sacrifice some tokens per frame to accommodate more frames. (b) Our progressive compression (PVC) achieves unified compression of images and videos, allowing for the continuous supplementation of image details and temporal dynamic information in subsequent frames.

markable success in various image-text tasks, demonstrating strong general capabilities. Many studies have further extended these models to handle both images and videos.

While videos can be seen as a natural extension of images over time, the additional temporal dimension poses new challenges. VLMs typically use visual tokens to represent visual information. A single image often requires hundreds or even thousands of tokens. If each frame of a video is encoded as an image in the same way, a 100-frame video would generate over tens of thousands of tokens, causing a significant computational burden during training and inference. To address this, VLMs use a technique called *visual token compression* [18, 59, 122] to reduce the number of tokens and lower computational complexity. The key challenge is finding a way to reduce the number of tokens while retaining essential information.

As shown in Fig. 1 (a), many high-performance VLMs usually process images and videos separately, using different visual token compression methods to meet the specific needs of each. For images, the models need to preserve fine-grained spatial details to support detail-intensive image tasks (e.g., OCR). For videos, current tasks often focus more on capturing dynamic changes over time and require fewer spatial details. This allows for fewer tokens per frame, sacrificing some spatial details to accommodate more frames. For example, Qwen2-VL [122] and LLaVA-OneVision [59] reduce the number of tokens per frame for videos compared to tokens per image to handle more frames. However, treating images and videos separately can hinder their combined capabilities, such as limiting the ability of video to recognize spatial details.

An ideal visual token compression method should support unified image and video processing, effectively capturing spatial details and temporal changes. To achieve this, as illustrated in Fig. 1 (b), we extend each image into a static video and introduce the concept of “progressive compression” for videos: the current frame only encodes new information not extracted from previous frames. This effectively reduces representation redundancy and lowers the number of tokens required for each frame. For the *video* modality, adjacent frames are often similar and naturally have temporal redundancy. Encoding each frame independently results in repeated information and wasted tokens. By applying progressive compression, token redundancy is minimized, and temporal changes can be captured efficiently. For the *image* modality, a single image is repeated into multiple frames to form a static video. Progressive compression can then be applied to these frames, allowing spatial details to be gradually supplemented in subsequent frames. This approach unifies the processing of images and videos. Even with a limited number of tokens per frame, spatial details and temporal changes can be preserved.

Specifically, our proposed *Progressive Visual Token Compression (PVC)* strategy is achieved with the following architectural designs: (1) We standardize VLM inputs as videos. Each image is repeated multiple times (4 times

by default) to form a “static” video. (2) A *progressive encoding module* is introduced to the vision encoder. This module consists of a causal temporal attention to avoid redundant information and progressively extract information complementary to the representations of previous frames. An AdaLN operator injected with timestep information is adopted to differentiate different frames and avoid redundant encoding. (3) An *adaptive compression module* is introduced to compress the visual tokens without redundancy. Based on PixelShuffle [112] with shared MLP (i.e., the token compression method used by the open-source VLM InternVL [18, 117]), we incorporate an additional AdaLN operator to extract different spatiotemporal information at different time steps.

We evaluate our model on a wide range of multi-modal benchmarks. Our model achieves state-of-the-art results across various video understanding benchmarks, including long video tasks (e.g., VideoMME [29], MLVU [153]) and fine-grained short video tasks (e.g., MVBench [64]). Meanwhile, on image understanding benchmarks, especially for detail-intensive tasks (e.g., DocVQA [93], InfoVQA [94]), our method incurs no performance loss. This demonstrates that unifying visual inputs into video format and leveraging temporal-based token encoding and compression enables large VLMs to better handle diverse visual tasks.

Our contributions can be summarized as follows:

- To address the limitations of separate image and video processing in existing VLMs, we propose *Progressive Visual Token Compression (PVC)* that unifies visual inputs as videos, which allows spatial details and temporal dynamics to be preserved across different modalities.
- We introduce a novel *progressive encoding module* and an *adaptive compression module* to progressively encode complement information in visual tokens. This effectively minimizes temporal redundancy while capturing essential spatiotemporal information, allowing a lower token-per-frame in our model.
- With the proposed progressive token compression, our model achieves state-of-the-art results across long video and fine-grained short video benchmarks. Meanwhile, it incurs no performance loss on image benchmarks, particularly in detail-sensitive tasks.

2. Related Work

Vision-Language Models for Images and Videos. In the realm of large vision-language models (VLMs), proprietary models [2, 97, 98, 116] and open-source models [4, 18, 19, 59, 60, 73, 74, 117, 122, 145] have demonstrated exceptional performance across a variety of visual scenarios, including single-image, multi-image, and video contexts. Large VLMs typically represent an image with hundreds or thousands of visual tokens, but the additional temporal dimension in videos leads to a considerable num-

ber of tokens, posing a great challenge. Some methods [75, 125, 146] extend the context length of the large language model to process more tokens, but this causes a huge computational burden during training and inference. Other methods use token compression techniques to reduce the number of tokens [59, 81, 122]. For instance, LLaVA-OneVision [59] spatially down-samples the video tokens by 2×2 ; Oryx MLLM [81] designs a dynamic compressor for different types of inputs, where videos are down-sampled to a smaller scale; Qwen2-VL [122] leverages pixel shuffle and 3D convs to down-sample vision tokens spatially and temporally, and reduces the resolution of video frames for long videos.

As mentioned above, existing methods usually compress image and video tokens with different strategies to meet the needs of different tasks, such as detailed images and long videos. Furthermore, the simple spatial or temporal down-sampling does not take full advantage of the temporal redundancy in videos, leading to an inefficient compression. Our approach, otherwise, unifies the inputs into videos and compresses tokens by exploiting the temporal redundancy.

Vision Transformer with Temporal Attention. Modern video encoders typically enhance the basic image encoder (e.g., Vision Transformer, ViT [25]) with temporal attention to account for the temporal correlations in videos. Video Swin Transformer [79] applies joint spatio-temporal attention within localized 3D windows. TimeSformer [7], ViViT [3], TESTA [102] and EVLGen [43] apply self-attention mechanism along the spatial and temporal dimensions, respectively. We also introduce an additional temporal attention module to ViT layers, but the attention is causal to realize progressive feature encoding. Besides, we replace the Layer Normalization with Adaptive Layer Normalization (AdaLN) injected with timestep conditions to avoid redundant encoding for different input frames.

Visual Token Compression. Visual token compression is commonly used in VLMs to reduce the number of vision tokens to fit in the context length of LLMs and reduce computational overhead. Applying pooling [86, 148], down-sampling [59, 134], or convolution [20] along the spatial and temporal dimensions is straightforward but may cause information loss. Many other works [4, 27, 63, 64, 76, 136, 144] employ Q-Former [61] that aggregates visual features into a fixed number of tokens with learnable queries. However, learning a cross-attention layer is more difficult, and the compressed tokens may lose spatial and temporal awareness. Current high-performance VLMs such as InternVL2 [117] and Qwen2-VL [122] leverage PixelShuffle that aggregates a local grid of tokens into a single one by concatenating along the feature dimension. Meanwhile, some works also devise token compression modules specifically for video inputs, for instance, spatio-temporal attentional pooling [104], and token selection based on the sim-

ilarity with text queries [65, 111]. Nevertheless, these approaches are not applicable to general image and video understanding tasks.

Our progressive compression is based on the high-performance PixelShuffle module. We incorporate AdaLN to extract different spatio-temporal information at different time steps to avoid redundant representation.

3. Method

3.1. Standardize Vision Inputs of VLMs as Videos

Current high-performance VLMs typically use different methods to compress image and video tokens. Due to limited computational budget, allocating more tokens per image is beneficial for understanding image spatial details, whereas video processing often involves sacrificing the number of tokens per frame to include more frames.

To address this dilemma, we standardize vision inputs of VLMs as videos, and apply the proposed progressive visual token compression for all videos. Specifically, each image is repeated into multiple frames to create a “static” video. Then, progressive compression allows LLMs to revisit the image multiple times and capture richer spatial information in subsequent static frames. This approach enables a unified visual token compression for images and videos, balancing the distinct needs of both modalities. Even when the number of tokens per frame is limited, the necessary spatial details and temporal dynamics can be gradually supplemented in subsequent frame tokens.

For each image x in the inputs, we repeat it T_{img} times to form a static frame sequence $[x, x, \dots, x]$ (by default $T_{\text{img}} = 4$). For each native video input, we uniformly sample T frames, where T is randomly chosen from the range of [16, 96] by default. In scenarios where dynamic resolution [18] is used, it is applied to every frame of both static and native videos.

3.2. Network Architecture

The network architecture for our proposed PVC is outlined in Fig. 2, comprising a Vision Transformer (ViT) with Progressive Encoding, an Adaptive Token Compression module, and a Large Language Model (LLM). To fully leverage the redundancy between video frames, we integrate temporal attention mechanism into the ViT for progressive encoding. Additionally, the adaptive compression module is introduced to effectively reduce the number of visual tokens per frame.

Vision Transformer with Progressive Encoding. To avoid redundant encoding of video frames and give the current frame the potential to only encode new information not extracted from previous frames, we add a temporal attention module within the ViT. To minimize overhead, temporal attentions are applied only in the last \tilde{L} layers of the ViT (with

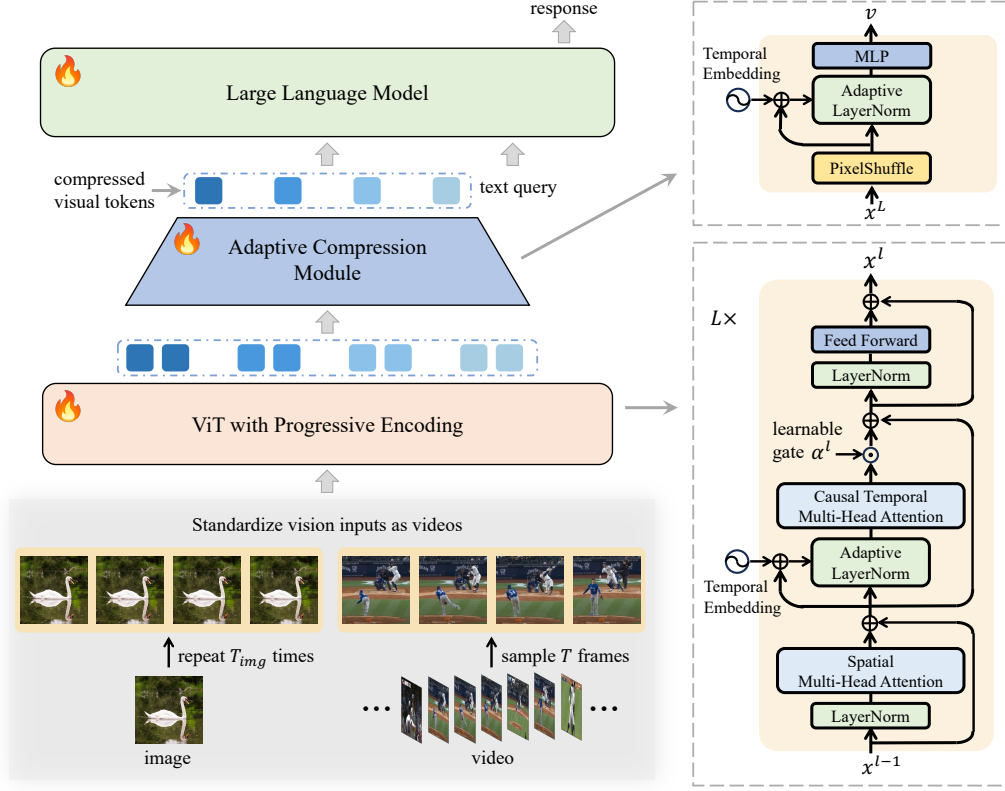


Figure 2. **Network architecture of progressive visual token compression (PVC)**. The inputs are standardized as videos, with images repeated to form static videos. A causal temporal attention and an AdaLN layer are incorporated into the ViT layers to progressively encode visual tokens across timesteps. The adaptive compression module, based on PixelShuffle, includes an AdaLN layer to reduce redundancy in visual tokens.

L layers in total). Let x be the video feature with dimensions $[B, T, N, C]$, where B is the batch size, T is the number of frames, N is the number of patches per frame, and C is the hidden dimension. The ViT layer with progressive encoding is defined by:

$$x := x + \text{S-MHA}(\text{LayerNorm}(x)), \quad (1)$$

$$x := x + \alpha \odot \text{T-MHA}(\text{AdaLN}(x; x + \text{TE})), \quad (2)$$

$$x := x + \text{FFN}(\text{LayerNorm}(x)). \quad (3)$$

Spatial Multi-Head Attention (S-MHA) is the original multi-head self-attention [118] in ViT, which is applied on the patch tokens of each frame respectively. x is reshaped to dimensions $[B \times T, N, C]$ when input into S-MHA, where N is the sequence length here.

Temporal Multi-Head Attention (T-MHA) is an additional causal multi-head self-attention [118] applied on the temporal dimension of the video feature. Each patch token attends to the tokens at the same spatial position in the previous frames. Specifically, x is rearranged to dimensions $[B \times N, T, C]$ when input into T-MHA, where T is the sequence length here.

Temporal Embedding (TE) is added to encode temporal position information. First, we use relative timestamps to

indicate the video frames: $t = [0, \frac{1}{T-1}, \dots, \frac{T-2}{T-1}, 1]$. Then we encode all timestamps by a 256-dimension sinusoidal position embeddings [118], denoted as $\tilde{t} \in \mathbb{R}^{T \times 256}$. After that, we obtain the temporal embedding via an MLP:

$$\text{TE} = W_2 \cdot \text{SiLU}(W_1 \tilde{t}) \quad (4)$$

where W_1 and W_2 are learnable parameters, SiLU refers to Sigmoid Linear Unit [35].

Adaptive Layer Normalization (AdaLN) was first proposed by [100] and is now widely used to adjust the normalization parameters according to given conditions, making the model more adaptable to different task requirements. In order to adapt to the ‘‘static’’ videos where different frames are the same, we use AdaLN here so that the network can extract different spatial information at different time steps and avoid redundant encoding. $\text{AdaLN}(x; z)$ normalizes the input x and applies an affine operation with the coefficients conditioned on z :

$$\text{AdaLN}(x; z) = \gamma(z) \odot \text{LayerNorm}(x) + \beta(z). \quad (5)$$

The affine scale $\gamma(z)$ and bias $\beta(z)$ are obtained via:

$$\gamma(z) = W_4 \cdot \text{SiLU}(W_3 z), \quad \beta(z) = W_6 \cdot \text{SiLU}(W_5 z), \quad (6)$$

where W_3, W_4, W_5 and W_6 are learnable parameters.

Additionally, a *learnable gate* $\alpha \in \mathbb{R}^C$ is introduced to scale the output of T-MHA. It is zero-initialized to make sure that the ViT is initialized as the pre-trained checkpoint.

Adaptive Compression. To reduce the computational budget, current VLMs [18, 59, 122] commonly shorten the sequence length by compressing visual tokens. For instance, InternVL-1.5 [18] employs a PixelShuffle [112] operation¹ followed by an MLP, reducing the visual token length by a factor of 4. However, this relies on a shared MLP to compress different visual sequences, which hinders reducing the representation redundancy between different frames.

To this end, we introduce an adaptive compression module by integrating an AdaLN [100] layer before the shared MLP. The reason for using AdaLN here is the same as in the progressive encoding module, allowing the network to extract different spatiotemporal information at different time steps to avoid redundant representation. The input of token compression is the output video tokens x with dimensions $[B, T, N, C]$ from the ViT. It compresses the number of tokens per frame from N to M as follows:

$$\tilde{x} = \text{PixelShuffle}(x) \in \mathbb{R}^{B \times T \times M \times (\frac{N}{M} \cdot C)} \quad (7)$$

$$v = \text{MLP}(\text{AdaLN}(\tilde{x}; \tilde{x} + \text{TE})). \quad (8)$$

where AdaLN and TE is the same as mentioned above.

By default, we set $M = \frac{1}{16}N$. Correspondingly, the kernel size for PixelShuffle is set to 4×4 , *i.e.*, it aggregates a 4×4 grid of tokens into a single token by concatenating along the feature dimension. Note that the compression ratio of 16 is higher than that in previous approaches (typically set to 4). For image modality, we repeat each image T_{img} times ($T_{\text{img}} = 4$ by default), resulting in the same visual token length as previous approaches for image input.

3.3. Training Strategies and Data

Training Strategies. Following common practices from previous VLMs [4, 18, 59, 74, 117, 122], the training of PVC consists of two stages: the pre-training stage and the instruction-tuning stage. The main difference is that all parameters of PVC are jointly trained in both stages, without freezing ViT or LLM as in previous approaches [4, 18, 59, 74, 117, 122]. We empirically find that this strategy works better for PVC (see Appendix for ablation experiments). Additionally, in the pre-training stage, we use a larger learning rate (10 \times) for randomly initialized parameters compared to pre-trained parameters.

Pre-training Data. The pre-training data used in PVC comprises two parts: (1) 45M image-text pairs used in InternVL2’s [117] pre-training stage, including LAION [105],

¹Originally from the super-pixel area [112]; here, it refers to concatenating 4 tokens from each adjacent 2×2 region along the channel dimension to form a single token.

COYO [9], *etc.* (2) 23M video-text pairs, including InternVid [127], WebVid [5], *etc.* The sampling ratio of image-text to video-text data is set to 1:1.

Instruction Tuning Data. The instruction tuning data used in PVC consists of two parts: (1) 7.2M image-text and video-text data used in InternVL2’s [117] fine-tuning stage. (2) 3.4M video-text data collected and refined from Vript [135], LLaVA-Video [151], *etc.* The sampling ratio of image-text to video-text data is set to 3:1.

For further details of training data, please refer to the Appendix. Note that all the image-text data used in PVC are adopted from InternVL2 [117], and we conduct experiments to assess the effect of the newly appended video-text data (see Appendix).

4. Experiment

4.1. Experiment Settings

Implementation Details. Our implementation mainly follows the InternVL series [18, 117], referred to as PVC_{InternVL2} below. We adopt ViT-L/14 [25] as the visual encoder, initializing its weights from InternViT-300M-448px-V1.5 [18]. The progressive encoding is introduced in the last 8 layers of the 24-layer ViT (*i.e.*, $\tilde{L} = 8$ and $L = 24$), whose T-MHA is randomly initialized. InternLM2-Chat-1.8B [10] is employed as the LLM for PVC_{InternVL2}-2B, while InternLM2.5-Chat-7B [10] is utilized for PVC_{InternVL2}-8B. We use the Adam optimizer [52] for both the pre-training and instruction-tuning stages, setting the learning rate to 2e-4 during pre-training and 4e-5 for fine-tuning. In the pre-training stage, the learning rate for weights initialized from pre-trained ViT and LLM models is reduced by a factor of 10 (*i.e.*, 2e-5). Weight decay is set to 0.01 in both stages. Our model is pre-trained on 50M samples and fine-tuned for 1 epoch. The input resolution for the visual encoder is set to 448×448 , with dynamic resolution [18] enabled for image data in both stages. The number of image tiles ranges up to 12, based on the image’s aspect ratio and resolution.

Evaluation Benchmarks. To validate PVC’s general capabilities, we evaluate it on various image-language and video-language benchmarks. The image-language benchmarks include AI2D [50], ChartQA [91], DocVQA [93], InfoVQA [94], SQA [83], TextVQA [113], MMB [78], MME [28], MMMU [142], SEED-I [58], and OCRBench [77]. For video-language benchmarks, we use MVBench [64], VideoMME [29], MLVU [153], LongVideoBench [131], NextQA [133], Egoschema [87], PercepTest [99], and ActNet-QA [139].

4.2. Comparison with State-of-the-art Methods

In this section, we evaluate our PVC across a wide range of multimodal benchmarks to validate its understanding and

Table 1. **Video-language benchmark results.** Our proposed PVC is compared with image-video general VLMs and video VLMs. “LongVideo.” refers to LongVideoBench. The results of VideoMME are reported as “without subscript/with subscript”. The best results among image-video general VLMs are **bold**, and the best results among all open-source VLMs are underlined. * Native resolution is used without fixed # token/frame. † 1024 tokens in total, with 16 or 96 frames used for different tasks.

| Model | Size | # token /frame | MVBench | VideoMME | MLVU | LongVideo. | NextQA | Egoschema | PercepTest | ActNet-QA |
|---------------------------------------|------|----------------------|-------------|-------------------|-------------|-------------|-------------|-------------|-------------|-------------|
| <i>Commercial VLMs:</i> | | | | | | | | | | |
| Gemini-1.5-Pro [116] | - | - | 52.6 | 75.0/81.3 | - | 64.0 | - | 64.5 | - | 57.5 |
| GPT-4V [97] | - | - | 43.7 | 59.9/63.3 | 49.2 | 61.3 | - | 55.6 | - | 57.0 |
| GPT-4o [98] | - | - | 47.8 | 71.9/77.2 | 64.6 | 66.7 | - | 72.2 | - | - |
| <i>Video VLMs:</i> | | | | | | | | | | |
| Video-CCAM [27] | 4B | 64/10.7 [†] | 62.8 | 50.1/51.2 | 56.5 | - | - | - | - | 58.0 |
| BLIP-3-Video [104] | 4B | 16 | - | - | - | - | 77.1 | - | - | 56.9 |
| VideoChat2 [64] | 7B | 96 | 60.4 | 39.5/43.8 | 47.9 | - | - | 54.4 | - | 49.1 |
| PLLaVA [134] | 7B | 144 | 46.6 | - | - | - | - | 54.5 | - | 56.3 |
| VideoLLaMA2 [20] | 7B | 72 | 54.6 | 47.9/50.3 | 48.5 | - | - | 51.7 | 51.4 | 50.2 |
| Tarsier [121] | 7B | 576 | 62.6 | - | - | - | 71.6 | 49.9 | 59.5 | - |
| LongVU [111] | 7B | 64-144 | 66.9 | -/60.6 | 65.4 | - | - | <u>67.6</u> | - | - |
| LLaVA-Video [151] | 7B | 169 | 58.6 | 63.3/ <u>69.7</u> | 70.8 | 58.2 | <u>83.2</u> | 57.3 | 67.9 | 56.5 |
| Kangaroo [75] | 8B | 1024 | 61.1 | 56.0/57.6 | 61.0 | 54.8 | - | 62.7 | - | - |
| InternVideo2 [128] | 8B | 96 | 67.2 | - | - | - | - | 60.0 | 63.4 | - |
| Video-CCAM [27] | 9B | 64/10.7 [†] | 64.6 | 50.3/52.6 | 58.5 | - | - | - | - | <u>59.7</u> |
| <i>Image-video general VLMs:</i> | | | | | | | | | | |
| Qwen2-VL [122] | 2B | -* | 63.2 | 55.6/60.4 | - | - | - | 54.9 | 53.9 | - |
| InternVL2 [117] | 2B | 256 | 60.2 | 45.0/47.3 | 50.4 | - | - | 46.7 | 49.9 | - |
| PVC_{InternVL2} (Ours) | 2B | 64 | 69.4 | 54.5/56.7 | 63.4 | 51.6 | 73.4 | 49.8 | 62.9 | 52.8 |
| LongVA [146] | 7B | 144 | - | 52.6/54.3 | 56.3 | - | 68.3 | - | - | 50.0 |
| IXC-2.5 [145] | 7B | 400 | 69.1 | 55.8/58.8 | 58.8 | - | 71.0 | - | 34.4 | 52.8 |
| LLaVA-OV [59] | 7B | 196 | 56.7 | 58.2/61.5 | 64.7 | 56.5 | 79.4 | 60.1 | 57.1 | 56.6 |
| Oryx MLLM [81] | 7B | -* | 63.9 | 58.3/62.6 | 67.5 | 55.3 | 81.9 | - | 68.6 | - |
| Qwen2-VL [122] | 7B | -* | 67.0 | 63.3/69.0 | - | - | - | 66.7 | 62.3 | - |
| InternVL2 [117] | 8B | 256 | 66.4 | 54.0/56.9 | 52.0 | - | - | 55.0 | 52.0 | - |
| PVC_{InternVL2} (Ours) | 8B | 64 | 73.8 | 64.1/69.7 | 72.4 | 59.2 | 82.0 | 59.6 | 68.4 | 57.1 |

reasoning abilities. We compare our PVC with state-of-the-art VLMs within 8B parameters, including commercial VLMs [97, 98, 116], open-source general VLMs [59, 81, 117, 122, 145, 146], and open-source video VLMs [20, 27, 64, 75, 104, 111, 121, 128, 134, 151]. As shown in Tab. 1 and Tab. 2, PVC achieves superior performance on long video tasks (e.g., VideoMME, MLVU) and fine-grained video tasks (e.g., MVBench), while maintaining very competitive performance on image tasks.

Video-Language Benchmarks. The results on video-language benchmarks are presented in Tab. 1, which can be summarized as the following:

(1) Our PVC_{InternVL2} utilizes 64 tokens per frame, which is

fewer than most existing methods (e.g., LLaVA-Video [151] uses 169 tokens, InternVL2 [117] uses 256 tokens). However, PVC_{InternVL2} achieves strong performance on all video tasks. In contrast, previous approaches such as LongVU [111] and VideoCCAM [27] also reduce tokens per frame to 64 but exhibit lower performance on the fine-grained video understanding task, MVBench. It demonstrates that our PVC can progressively capture the information from video frames and effectively exploit the temporal redundancy (see the ablation study in Tab 3 for evidence.)

(2) Our PVC_{InternVL2}-8B attains superior performance on MVBench, VideoMME, MLVU, and LongVideoBench, demonstrating its strong capability in both fine-grained

Table 2. **Image-language benchmark results.** We compare our PVC with VLMs that support both image and video inputs. * Native resolution is used without fixed # token/image tile.

| Model | Size | # token /image tile | AI2D | ChartQA | DocVQA | InfoVQA | SQA | TextVQA | MMB | MME | MMMU | SEED-I | OCRBench |
|---------------------------------------|------|---------------------|-------------|-------------|-------------|-------------|-------------|-------------|-------------|-------------|-------------|-------------|------------|
| | | | test | test | test | test | test | val | en-test | sum | val | - | - |
| <i>Commercial VLMs:</i> | | | | | | | | | | | | | |
| Gemini-1.5-Pro [116] | - | - | 94.4 | 87.2 | 93.1 | 81.0 | - | - | - | - | 62.2 | - | - |
| GPT-4V [97] | - | - | 78.2 | 78.5 | 88.4 | - | 75.7 | - | - | 1926 | 56.8 | 49.9 | - |
| GPT-4o [98] | - | - | 94.2 | 85.7 | 92.8 | - | - | - | 83.4 | 2329 | 69.1 | 76.2 | 736 |
| <i>Image-video general VLMs:</i> | | | | | | | | | | | | | |
| Qwen2-VL [122] | 2B | -* | 74.7 | 73.5 | 90.1 | 65.5 | - | 79.7 | 74.9 | 1872 | 41.1 | - | 809 |
| InternVL2 [117] | 2B | 256 | 74.1 | 76.2 | 86.9 | 58.9 | 94.0 | 73.4 | 73.2 | 1877 | 34.3 | 71.6 | 784 |
| PVC_{InternVL2} (Ours) | 2B | 64 | 76.3 | 78.9 | 87.7 | 59.9 | 94.9 | 76.2 | 75.8 | 1960 | 36.9 | 73.2 | 796 |
| LongVA [146] | 7B | 144 | 70.7 | 70.4 | 80.8 | 49.4 | - | - | - | - | 42.6 | - | - |
| IXC-2.5 [145] | 7B | 400 | 81.5 | 82.2 | 90.9 | 69.9 | - | 78.2 | 82.2 | 2229 | 42.9 | 75.4 | 690 |
| LLaVA-OV [59] | 7B | 729 | 81.4 | 80.0 | 87.5 | 68.8 | 96.0 | - | - | 1998 | 48.8 | 75.4 | - |
| Oryx MLLM [81] | 7B | -* | 78.5 | - | 89.0 | - | - | 75.0 | 81.4 | - | 43.9 | - | 672 |
| Qwen2-VL [122] | 7B | -* | 83.0 | 83.0 | 94.5 | 76.5 | - | 84.3 | 83.0 | 2327 | 54.1 | - | 866 |
| InternVL2 [117] | 8B | 256 | 83.8 | 83.3 | 91.6 | 74.8 | 97.1 | 77.4 | 81.7 | 2210 | 49.3 | 76.2 | 794 |
| PVC_{InternVL2} (Ours) | 8B | 64 | 83.8 | 84.1 | 92.5 | 75.0 | 97.7 | 80.0 | 83.9 | 2282 | 50.9 | 77.2 | 807 |

and long video understanding. Notably, PVC_{InternVL2-8B} reaches 73.8 on MVBench, significantly surpassing the previous best accuracy of 69.1 among open-source models within 8B parameters, set by IXC-2.5 [145].

(3) Our PVC_{InternVL2-8B} also obtains the best results in NextQA and ActNet-QA among image-video general VLMs. On Egoschema and PercepTest, our model is inferior to some existing models, which may be caused by the lack of training data in some specific domains.

Image-Language Benchmarks. The results on image-language benchmarks are presented in Tab. 2 and can be summarized as follows:

(1) PVC_{InternVL2} uses the same architecture and image-text training data as InternVL2 [117]. In comparison with InternVL2, PVC_{InternVL2} does not compromise performance on image tasks, even on OCR-related tasks (*e.g.*, DocVQA, InfoVQA, *etc.*) that heavily depend on spatial details (as shown in Tab. 3, directly reducing the tokens per patch would significantly hurt performance on DocVQA and InfoVQA). This validates that PVC can progressively encode spatial information from repeated images through the temporal attention module, and effectively compress the visual tokens to fully preserve spatial details. Notably, PVC_{InternVL2-8B} improves TextVQA performance from 77.4 to 80.0 (+2.6).

(2) Compared to Qwen2-VL-7B [122], our PVC_{InternVL2-8B} achieves comparable or better performance on AI2D (+0.8), ChartQA (+1.1), and MMB (+0.9), but lags behind on DocVQA (-2.0), InfoVQA (-1.5), TextVQA (-4.3), MME (-45), MMMU (-3.2), and OCRBench (-59). The benchmarks

where Qwen2-VL excels are primarily OCR-related (4 out of 6), which are highly sensitive to OCR-specific training data. Given the differences in model architecture and training data, a direct comparison is challenging. However, our PVC is orthogonal and complementary to the advances in model architecture and training data. The ablation studies in Tab. 3 show the effectiveness of our PVC.

4.3. Ablation Study

In this section, we present a series of ablation experiments to validate the effectiveness of PVC. To reduce experimental burden, the ablation study is conducted on 2B model with shortened pre-training on 10M samples. Different ablation settings are evaluated on representative video-language benchmarks (MVBench, VideoMME, and MLVU) and image-language benchmarks (DocVQA, InfoVQA, and MMB). The results are presented in Tab. 3.

Standardize Vision Inputs as Videos. The standardization reduces tokens per image from 256 to 64 while maintaining the overall number of visual tokens by repeating each image and increasing the number of video frames. As shown in settings (a) and (b) of Tab. 3, directly standardizing vision inputs as video significantly reduces performance on OCR-related image tasks (DocVQA -3.7 and InfoVQA -6.5) and fine-grained video tasks (MVBench -3.9). This performance drop occurs because repeating the image four times for the vanilla ViT and vision compression module only produces four groups of identical visual tokens, with repeated information encoded. Consequently, spatial details are lost compared to using 256 distinct visual tokens. How-

Table 3. **Ablation of key components in PVC.** The ablation study is conducted on 2B model with shortened pre-training on 10M samples. “Adapt. compress” refers to adaptive compression. VideoMME is tested under “without subscript” setting.

| Settings | # tokens per image | # image repeat | # video frames | Progressive encoding | Adapt. compress | MVBench | VideoMME | MLVU | DocVQA | InfoVQA | MMB |
|----------|--------------------|----------------|----------------|----------------------|-----------------|---------|----------|------|--------|---------|------|
| (a) | 256 | 1 | 16 | | | 61.9 | 44.9 | 50.5 | 86.4 | 59.1 | 75.1 |
| (b) | 64 | 4 | 64 | | | 58.0 | 46.0 | 53.0 | 82.7 | 52.6 | 73.1 |
| (c) | 64 | 4 | 64 | ✓ | | 61.8 | 46.5 | 54.2 | 85.9 | 58.1 | 74.8 |
| PVC | 64 | 4 | 64 | ✓ | ✓ | 62.4 | 46.7 | 55.1 | 86.7 | 58.5 | 74.9 |

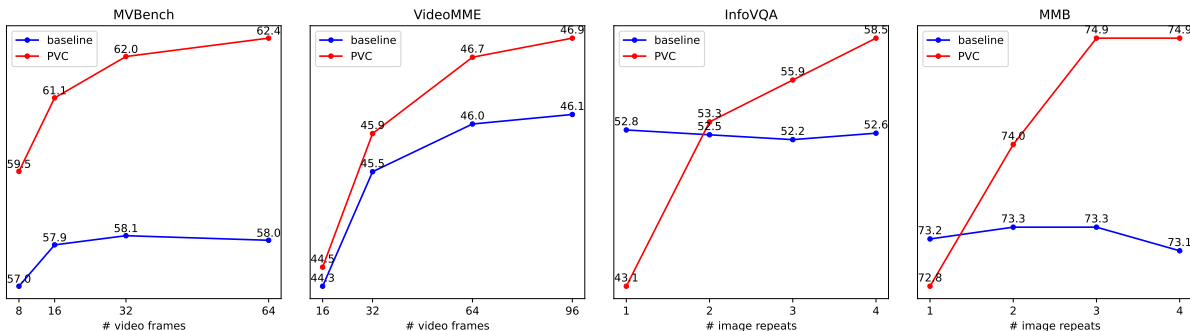


Figure 3. **Analysis of progressive compression.** We compare our PVC model with the baseline without progressive compression (setting (b)) in Tab. 3. For video tasks (MVBench and VideoMME), we test different number of input frames. For image tasks (InfoVQA and MMB), we test different repetition times of the image.

ever, long-video understanding tasks (VideoMME +1.1 and MLVU +2.5), which do not require as much visual detail, can benefit from the increase in video frames.

Progressive Encoding. Progressive encoding involves adding temporal causal attention in ViT. As shown in Tab. 3, settings (b) and (c) demonstrate that adding temporal attention in ViT mitigates the information loss observed in setting (a) and maintains comparable performance with setting (a) on tasks requiring spatial details (MVBench, DocVQA, and InfoVQA). Furthermore, temporal attention significantly boosts performance on long video tasks (MLVU +1.2 and VideoMME +0.5). These results validate that our proposed progressive encoding techniques can effectively encode both spatial details and temporal correlations.

Adaptive Compression. As shown in Tab. 3 setting (c) and PVC, the performance on all tasks is further improved by adding the adaptive compression module, especially on long video tasks (e.g., MLVU +0.9). This demonstrates our proposed adaptive compression mechanism can better exploit representation redundancy within video frames and model long-term temporal correlations.

4.4. Analysis

Effectiveness of Progressive Compression. We evaluate our model by gradually increasing the number of video frames and image repetitions. We use the model in Tab. 3 setting (b) (without progressive compression) as the baseline. The results are shown in Fig. 3.

For MVBench, which mainly contains videos shorter than one minute with fine-grained queries, the baseline

Table 4. **Speed of image repetition and progressive encoding.** We report the FLOPs and FPS (samples per second) for processing samples containing a 448×448 image and 2048 text tokens, measured on an NVIDIA A100.

| Model | # tokens per image | # image repeats | Progressive encoding | FLOPs | FPS |
|-----------------------------|--------------------|-----------------|----------------------|-------|-------|
| InternVL2-8B | 256 | 1 | | 13.3T | 4.8 |
| PVC _{InternVL2-8B} | 64 | 4 | ✓ | 14.1T | 4.5 |
| Δ_{relative} | - | - | - | +6.0% | -6.3% |

model’s score plateaus after increasing to 16 frames, while our model still gets better with complement information encoded. For the long-video task VideoMME, the scores of both models increase with the number of frames. Still, our model grows faster, indicating that it is better at removing temporal redundancy and capturing temporal dynamics.

On image tasks, increasing the number of image repetitions does not boost the baseline model’s performance since its repeated visual tokens do not provide more information. On the detail-sensitive task InfoVQA, our model performs poorly when the image is repeated only once because only part of the information is extracted. When the image is repeated more times, the detailed information is supplemented, so the results get substantially better. For MMB, the images contain less spatial details, so the gain from repeating more times is relatively small for our model.

Speed of Image Repetition and Progressive Encoding.

As shown in Tab. 4, for the 8B model, repeating images introduces only a marginal overhead (+6.0% FLOPs relative, -6.3% FPS relative), since the visual feature computation

can be partially reused and the main computational load is in the LLM. Thus, the inference speed of our PVC_{InternVL2} on image tasks remains similar to that of InternVL2.

5. Conclusion

In conclusion, our work introduces Progressive Visual Token Compression (PVC), a unified approach for effectively processing images and videos within large Vision-Language Models (VLMs). This strategy leverages the standardization of visual inputs as videos, alongside a progressive encoding module and an adaptive compression module. Extensive empirical analysis demonstrates that PVC can gradually capture both spatial details and temporal dynamics from the sequence of image repetitions and video frames. Consequently, PVC not only unifies image and video processing, but also achieves state-of-the-art performance on fine-grained short video tasks and long video tasks. It also maintains accuracy on image benchmarks, particularly in detail-sensitive tasks.

Acknowledgments. This work is supported by the National Key R&D Program of China (NO. 2022ZD0161300), by the National Natural Science Foundation of China (62376134).

Appendix

A. Training Details

Hyper-parameters used in the pre-training and instruction tuning of PVC are listed in Tab. 5.

Table 5. Training hyper-parameters of PVC.

| Training stage | Pre-training | Instruction tuning |
|-------------------------|---------------------------------|--------------------|
| Max sequence length | 8192 | |
| Max tile/image | 12 | |
| Token/frame (tile) | 64 | |
| Number of image repeats | 4 | |
| Number of video frames | 16-96, uniform | |
| Optimizer | AdamW | |
| Learning rate | 2e-4 | 4e-5 |
| Weight decay | 0.01 (2B), 0.05 (8B) | |
| Optimizer momentum | $\beta_1, \beta_2 = 0.9, 0.999$ | |
| Learning rate schedule | constant with warmup | cosine decay |
| Warmup steps | 100 | 240 |
| Training steps | 25k | 8k |
| Batch size | 2048 | 1024 |

B. Dataset Details

The data used in the pre-training stage are listed in Tab 6. All image-text data is adopted from InternVL2 [117]. For video datasets, we initially utilize large-scale but mixed-quality datasets including InternVid-10M [127], WebVid-10M [5], TextVR [132] and OpenVid-1M [96] that primar-

Table 6. Summary of datasets used in the pre-training stage.

*IT refers to the instruction tuning data in VideoChat2.

| task | dataset |
|---------------|--|
| Short Caption | Laion (en&zh) [105], COYO [9], COCO [67] |
| OCR | Wukong-OCR [31], LaionCOCO-OCR [106] |
| Detection | GRIT [101], Objects365 [110] |
| Conversation | All-Seeing (en&zh) [123] |

Image-text instruction data (see Tab. 7a)

(a) Image-text datasets used in the pre-training stage.

| task | dataset |
|------------------|---|
| Short Caption | InternVid-10M [127], WebVid [5], OpenVid [96], TextVR [132] |
| Detailed Caption | MiraData [45], ShareGPT4Video [17], Vript [135], Vript_Chinese [135], LSMDC [103] |
| VQA | STAR [129], VideoGPT+ [85], EgoTaskQA [42], CLEVRER [137], Mementos [126] |
| Classification | NTU RGB+D [109] |
| Comprehensive | VideoChat2-IT* [64], FineVideo [26] |

(b) Video-text datasets used in the pre-training stage.

Table 7. Summary of datasets used in the instruction tuning stage. *IT refers to the instruction tuning data in VideoChat2.

| task | dataset |
|--------------|---|
| General QA | VQAv2 [30], GQA [41], OKVQA [89], VSR [70] |
| Science | AI2D [50], ScienceQA [83], Chemistry Data [62], TQA [51] |
| Medical | PMC-VQA [149], VQA-RAD [55], VQA-Med [6], Medical-Diff-VQA [38], PathVQA [34], SLAKE [68], PMC-CaseReport [130] |
| Chart | ChartQA [91], LRV-Instruction [71], PlotQA [95], Unichart [92], MMC-Inst [72], DVQA [46], TableMWP [84], FigureQA [47], MapQA [13], SciTSR [21], Fintabnet [152] |
| Mathematics | CLEVR [44], MetaMath [138], GeoQA+ [11], Geometry3k [82], GeoS [107], Unigeo [15], Super-CLEVR [66], MathQA [1] |
| Knowledge | Art500k [88], MovieNet [39], KonIQ-10k [36], KVQA [108], ViQuAE [57] |
| OCR | InfoVQA [94], TextVQA [113], ArT [22], CASIA [69], Chart-to-text [48], COCO-text [119], CTW [140], EATEN [32], ICDAR2019-LSVT [115], ICPR MTWI [33], NAF [24], ReCTS [147], TextOCR [114], LLaVAR [150], HME-100k [141], POIE [53], SROIE [40], ST-VQA [8], EST-VQA [124], IAM [90] |
| Document | DocVQA [23], DocReason25k [37] |
| Grounding | RefCOCO [49], RefCOCO+ [49], RefCOCOg [49], RD-BoxCoT [16] |
| Conversation | ALLaVA [14], LAION-GPT4V [54], MMDU [80], TextOCR-GPT4V [12] |
| Detection | Objects365 [110], V3Det [120] |

(a) Image-text datasets used in the instruction tuning stage.

| task | dataset |
|------------------|--|
| Detailed Caption | ShareGPT4Video (en&zh) [17], Vript_Chinese [135], Vript [135], LSMDC [103] |
| VQA | STAR [129], EgoTaskQA [42], Mementos [126], TVQA [56], HiREST [143], PerceptionTest [99] |
| Classification | NTU RGB+D [109] |
| Comprehensive | VideoChat2-IT* [64], LLaVA-Video [151] |

(b) Video-text datasets used in the instruction tuning stage.

Table 8. **Ablation of the training data.** "New data" refers to our training dataset, which combines newly collected video-text data with InternVL2's data. Otherwise, the model is trained solely with InternVL2's data.

| Model | New data | MVBench | VideoMME | MLVU | DocVQA | InfoVQA | MMB |
|-----------------------------|----------|---------|----------|------|--------|---------|------|
| InternVL2-2B | | 60.2 | 45.0 | 50.2 | 86.9 | 58.9 | 73.2 |
| PVC _{InternVL2-2B} | | 62.0 | 47.7 | 54.1 | 87.8 | 59.6 | 75.3 |
| PVC _{InternVL2-2B} | ✓ | 69.4 | 54.5 | 63.4 | 87.7 | 59.9 | 75.8 |

Table 9. **Ablation of the training strategy.** The ablation study is conducted on 2B model with shortened pre-training on 10M samples. "Unfreeze ViT & LLM" means unfreezing the parameters of the ViT and LLM during the pre-training stage with a lower learning rate ($\times 0.1$). * InternVL2 model is trained under our ablation setting.

| Model | Unfreeze ViT & LLM | MVBench | VideoMME | MLVU | DocVQA | InfoVQA | MMB |
|--------------------------|--------------------|---------|----------|------|--------|---------|------|
| InternVL2* | | 60.9 | 44.7 | 50.0 | 86.1 | 58.7 | 74.2 |
| InternVL2* | ✓ | 61.9 | 44.9 | 50.5 | 86.4 | 59.1 | 75.1 |
| PVC _{InternVL2} | | 60.6 | 45.5 | 53.2 | 84.8 | 57.3 | 74.4 |
| PVC _{InternVL2} | ✓ | 62.4 | 46.7 | 55.1 | 86.7 | 58.5 | 74.9 |

ily feature short video captions. To enhance the model's understanding of visual details, we further incorporate densely captioned video-text datasets of varied video lengths including MiraData [45], ShareGPT4Video [17] and the Vript series [135]. To improve capabilities in multi-turn conversation and visual reasoning, we employ VideoGPT+ [85], STAR [129], EgoTaskQA [42], CLEVRER [137] and Mementos [126]. Additionally, NTU RGB+D [109] is used to boost robustness to action recognition. Lastly, to enhance the model's holistic abilities, we utilize comprehensive datasets VideoChat2-IT [64] and FineVideo [26], which aggregate elements of multiple-choice answering, open-ended question-answering, and conversations.

Datasets used for instruction tuning are listed in Tab 7. The image-text data is also adopted from InternVL2 [117]. For video-text data, low-quality datasets used in the pre-training stage are replaced by compositional high-quality datasets like LSMDC [103], TVQA [56], HiREST [143] and LLaVA-Video [151].

C. Appended Ablation Studies

C.1. Training Data

To further assess the effect of the newly appended video-text data, we train a PVC_{InternVL2} model with the original training data of InternVL2 [117]. The results are reported in Tab. 8.

(1) In a fair comparison with InternVL2, our PVC achieves comparable or superior performance on image benchmarks, confirming that our proposed progressive encoding effectively preserves spatial details in images. On video benchmarks, especially for long video tasks (e.g., VideoMME and MLVU), our PVC outperforms InternVL2 by a large margin. This is because our PVC can process more video frames with a lower token-per-frame and better capture the

temporal correlations in videos with progressive encoding.

(2) For our PVC, incorporating the new video-text data significantly improves performance on video tasks while maintaining the performance on image tasks.

In conclusion, the significant improvements on video tasks is attributed to our PVC's strong ability to capture spatiotemporal information in videos, as well as the enhanced quality and diversity of the dataset contributed by the newly added video data. Ablation studies in Tab. 3 and fair comparisons with InternVL2 in Tab. 8 have demonstrated that our PVC attains great improvements in video understanding. Meanwhile, current high-performing VLMs for videos, such as Qwen2-VL [122] and LLaVA-Video [151], rely on high-quality video data, which is relatively scarce in the original dataset of InternVL2. To address this, we incorporate recently released open-source video data (e.g., LLaVA-Video [151]), further elevating our PVC to state-of-the-art performance.

Moreover, the stable performance on image benchmarks further validates the robustness of our progressive encoding approach. While the newly introduced data is tailored to video understanding, our PVC's ability to generalize across modalities ensures that improvements on video tasks do not come at the expense of degrading performances on image tasks. This underscores the versatility of our method in handling multi-modal inputs and highlights the complementary roles of methodology and data in driving performance improvements.

C.2. Training Strategy

During the pre-training phase, we unfreeze the parameters of the ViT and LLM, which differs from existing methods [4, 18, 59, 74, 117, 122]. The ablation results in the Tab. 9 empirically explain why we adopt this training strat-

egy. For InternVL2, keeping ViT and LLM fixed or trainable during pre-training has minimal impact on the final performance. However, for our PVC, unfreezing the ViT and LLM during pre-training leads to significantly better performances. We suppose this improvement is due to the following reasons: (1) Training the ViT jointly with the newly added progressive encoding module enables better capture of complementary information and minimizes redundancy. (2) The LLM’s inherent capability to process multi-frame videos is limited, especially for integrating different information extracted from the repeated frames of an image. Thus, additional training is needed for effective adaptation.

C.3. Conditions of AdaLN

We ablate the conditions used in the AdaLN layer, and the results are listed in Tab. 10. Without any condition, AdaLN degrades to LN layer. Repeated frames of the images lack distinct timestep indicators, resulting in redundant encoding and poor performance. Introducing temporal embedding (TE) as the condition significantly boosts the performances. Adding the feature x to the condition provides further improvements. x contains temporal information aggregated from previous layers, which helps better extract complementary information and minimize redundancy.

Table 10. **Ablation of conditions of AdaLN layers.** The ablation study is conducted on 2B model with shortened pre-training on 10M samples.

| AdaLN condition | MVBench | VideoMME | InfoVQA | MMB |
|-----------------|---------|----------|---------|------|
| - | 59.2 | 46.4 | 54.0 | 73.7 |
| TE | 62.0 | 46.5 | 57.8 | 74.6 |
| $x + TE$ | 62.4 | 46.7 | 58.5 | 74.9 |

C.4. Number of Temporal Attention Layers

As described in Sec.3.2, we add temporal attention to the last \tilde{L} layers of the ViT. As shown in Tab. 11, $\tilde{L} = 8$ performs better than $\tilde{L} = 1$ or $\tilde{L} = 4$. Setting $\tilde{L} = 24$ (adding temporal attention to each layer) does not provide significant improvements over $\tilde{L} = 8$ but increases computational overhead. Therefore, we choose $\tilde{L} = 8$, *i.e.*, adding temporal attention to the last 8 layers of the ViT.

D. Qualitative Results

Image Progressive Encoding. As shown in Fig. 4, when an image is repeated as multiple frames, our PVC can extract more precise details and supplementary information from the subsequent frames. For instance, the model extracts the title “Goal 15 life on land” from the first frame and corresponding detailed goals from subsequent frames. Incorrect contents, *e.g.* “10% of the total land area”, are also corrected using the information extracted from subsequent frames.

Table 11. **Ablation of the number of temporal attention layers in ViT.** The ablation study is conducted on 2B model with shortened pre-training on 10M samples.

| # temp. attn. layer (\tilde{L}) | MVBench | VideoMME | InfoVQA | MMB |
|-------------------------------------|---------|----------|---------|------|
| 1 | 61.6 | 46.3 | 55.8 | 74.2 |
| 4 | 62.1 | 46.6 | 57.3 | 74.7 |
| 8 | 62.4 | 46.7 | 58.5 | 74.9 |
| 24 | 62.5 | 46.7 | 58.8 | 74.8 |

Video Dynamic Capture. As shown in Fig. 5, the video contains several consecutive collisions, testing the model’s ability to capture spatiotemporal dynamics. InternVL2 [117] describes each collision moment independently but lacks a description of the whole process and includes inaccuracies. LLaVA-OneVision [59] and Qwen2-VL [122] exhibit numerous errors when capturing object interactions. In contrast, our PVC not only accurately describes the process of each collision and the associated object movements but also identifies the causal relationships between multiple collisions.

Image Progressive Encoding



User: What is the content in this picture?

PVC (image repeat × 1):

The image is an infographic related to Sustainable Development Goal 15, which focuses on Life on Land. It highlights the importance of forests in Indonesia and the challenges they face. Here is a detailed breakdown of the content:

- Title and Header**
- SDGs FACTSHEET
 - INDONESIA
 - GOAL 15
 - LIFE ON LAND

Key Points

- 1. Forest Area**
 - There are 91 million hectares of forests in Indonesia, covering just over **10%** of the total land area.
- 2. Archipelagic and State Forests**
 - Indonesia is home to the third largest tropical forests, which are essential for the livelihood of 48.8 million Indonesians. These **forests cover 14.9 million hectares, or nearly 8%** of Indonesia's total land area.
- 3. Biodiversity**
 - Tropical forests are home to important biodiversity, providing a highly effective natural terrestrial carbon storage system.
- 4. Mangrove Forests**
 - Mangrove forests provide multiple ecosystem services, including fishery resources, coastal protection, and biodiversity support.
- 5. Land Use and Emissions**
 - In 2005, 63% of emissions were the result of land use change and peatland degradation. Mangrove forests are also threatened.
- 6. Deforestation and Loss**
 - The average annual net loss of forest is 685,000 hectares. Forests are lost through deforestation, biodiversity loss, and affecting the livelihoods of forest-dependent communities.
- 7. Future Goals**
 - By 2030, Indonesia aims to restore 2 million hectares of degraded peatland ecosystems.

Visual Elements

- **Icons:** The infographic uses icons of trees, forests, and other related imagery to visually represent the information.
- **Colors:** Predominantly green, symbolizing nature and forests, with white and brown accents for text and details.

Conclusion

The infographic emphasizes the critical role of forests in Indonesia, the threats they face, and the country's efforts to address these issues through sustainable practices and restoration goals.

PVC (image repeat × 4):

The image is an infographic related to Goal 15 of the Sustainable Development Goals (SDGs), which focuses on Life on Land. The infographic provides information about Indonesia's forests and peatlands, emphasizing the importance of forest conservation and restoration. Here is a detailed breakdown of the content:

- Title and Goal**
- SDGs FACTSHEET
 - INDONESIA
 - Goal 15: Life on Land

Key Points

- 1. Forest Area**
 - There are 91 million hectares of forests in Indonesia, covering just over **half** of the country's total land area.
- 2. Archipelagic and State by Area**
 - **Indonesia is the largest archipelagic and 15th biggest state by area in the world. It has a significant impact on the world's climate conditions.**
- 3. Dependence on Forests**
 - Indonesia is home to the third largest tropical forests. 48.8 million people in Indonesia directly depend on forest (or forest ecosystem services) for their livelihood.
- 4. Peatlands**
 - **Peatlands cover an estimated 14.9 million hectares, or nearly 8%**, of Indonesia's total land area. Tropical peatlands are home to important biodiversity and a highly effective natural terrestrial carbon storage system.
- 5. Mangrove Forests**
 - **Indonesia is home to more than 20% (2.2 million hectares) of the world's mangrove forests.** Mangrove forest ecosystems nurture fishery and forest resources, mitigate coastal disasters, and climate change, provide multiple ecosystem services, and eco-tourism opportunities, and accommodate biodiversity.
- 6. Emissions and Degradation**
 - In 2005, 63% of emissions were the result of land use change and **peat fires**.
 - The average annual net loss of forest **between 2010 and 2015** was 685,000 hectares. Forests are lost through deforestation, **endangering globally important biodiversity** and affecting the livelihoods of forest-dependent communities.
- 7. Future Goals**
 - By 2030, Indonesia aims to restore 2 million hectares of degraded peatland ecosystems.

Visual Elements

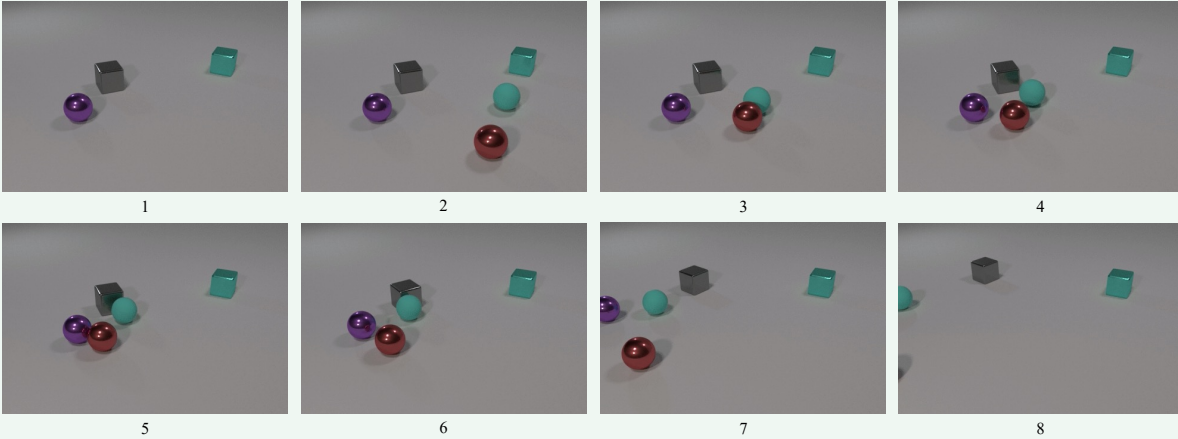
- The infographic includes icons of trees, forests, and peatlands.
- It uses a green color scheme to emphasize the environmental focus.
- **The United Nations Sustainable Development Goals logo is present at the bottom left.**

Conclusion

The infographic highlights the critical role of forests and peatlands in Indonesia, emphasizing the need for sustainable forest management and restoration to combat deforestation, land degradation, and biodiversity loss. It underscores the interdependence of local communities on forest ecosystems and the global impact of Indonesia's forests on climate conditions.

Figure 4. PVC achieves image progressive encoding. The image is repeated once (left) and four times (right). Supplementary contents are marked in blue, incorrect contents in red, and corrected contents in green.

Video Dynamic Capture



User: Describe the collisions in the video in detail.

InternVL2-8B:

In the video, the **purple metal sphere and the red metal sphere collide**. The **red metal sphere and the cyan rubber sphere collide**. The **gray metal cube and the cyan rubber sphere collide**. The **gray metal cube and the red metal sphere collide**.

LLaVA-OneVision-7B:

The video shows a sequence of geometric shapes, specifically spheres and cubes, that are arranged on a flat surface. The shapes come in different colors: purple, red, cyan, and gray. The objects move around the surface, with some colliding with each other. Starting from the beginning, there is a single purple sphere visible. As the video progresses, more objects appear, including a red sphere, a gray cube, and a cyan sphere. The objects move independently for a while before they start to interact. One notable collision occurs when **the gray cube collides with the cyan sphere**. This collision causes both objects to change their positions slightly. Following this, **the red sphere moves towards the gray cube and appears to make contact**, causing **the gray cube to shift position again**. The video continues with **the red sphere moving away from the gray cube and the cyan sphere remaining stationary**. The **purple sphere** is also visible but **does not seem to be involved in any collisions** at this point. Towards the end of the video, **the red sphere moves closer to the gray cube once more**, and it looks like it might collide with it again. However, **the red sphere stops short of making contact**, leaving the gray cube in its original position.

Qwen2-VL-7B:

The video shows a sequence of collisions between different colored spheres and cubes on a flat surface. Initially, there are three objects: a purple metallic sphere, a gray metallic cube, and a cyan metallic cube. A cyan rubber sphere enters the scene and **collides with the purple sphere**. The **purple sphere then collides with the gray cube**. The **cyan rubber sphere collides with the red metallic sphere**, which **then collides with the purple sphere**. The **purple sphere collides with the gray cube**. The **cyan rubber sphere collides with the gray cube**. **The red metallic sphere collides with the gray cube**.

PVC-8B (ours):

The video shows a series of interactions between different objects. Initially, there are three objects: a purple sphere, a gray cube, and a cyan cube. The **purple sphere and the gray cube are stationary**. Then, a red sphere enters the scene and **collides with the cyan sphere**, causing the cyan sphere to move away. The red sphere continues to move and eventually collides with the purple sphere, causing the purple sphere to move. The gray cube also moves slightly due to the collision with the cyan sphere. Finally, the red sphere and the cyan sphere exit the scene, **leaving the gray cube in its new position**.

Figure 5. **PVC effectively captures spatiotemporal dynamics in videos.** Correct descriptions of the movements and interactions of the objects are marked in **blue**, while incorrect descriptions are marked in **red**. For visualization, we select the above 8 key frames from the video, while the entire video is fed into the models.

References

- [1] Aida Amini, Saadia Gabriel, Peter Lin, Rik Koncel-Kedziorski, Yejin Choi, and Hannaneh Hajishirzi. Mathqa: Towards interpretable math word problem solving with operation-based formalisms. *arXiv preprint arXiv:1905.13319*, 2019. 9
- [2] Anthropic. Claude 3.5 sonnet, 2024. 1, 2
- [3] Anurag Arnab, Mostafa Dehghani, Georg Heigold, Chen Sun, Mario Lučić, and Cordelia Schmid. Vivit: A video vision transformer. In *ICCV*, pages 6836–6846, 2021. 3
- [4] Jinze Bai, Shuai Bai, Shusheng Yang, Shijie Wang, Sinan Tan, Peng Wang, Junyang Lin, Chang Zhou, and Jingren Zhou. Qwen-vl: A versatile vision-language model for understanding, localization, text reading, and beyond. *arXiv preprint arXiv:2308.12966*, 1(2):3, 2023. 1, 2, 3, 5, 10
- [5] Max Bain, Arsha Nagrani, Gül Varol, and Andrew Zisserman. Frozen in time: A joint video and image encoder for end-to-end retrieval. In *ICCV*, pages 1728–1738, 2021. 5, 9
- [6] Asma Ben Abacha, Sadid A Hasan, Vivek V Datla, Dina Demner-Fushman, and Henning Müller. Vqa-med: Overview of the medical visual question answering task at imageclef 2019. In *Proceedings of CLEF (Conference and Labs of the Evaluation Forum) 2019 Working Notes*. 9-12 September 2019, 2019. 9
- [7] Gedas Bertasius, Heng Wang, and Lorenzo Torresani. Is space-time attention all you need for video understanding? In *ICML*, page 4, 2021. 3
- [8] Ali Furkan Biten, Ruben Tito, Andres Mafla, Lluís Gomez, Marçal Rusinol, Ernest Valveny, CV Jawahar, and Dimosthenis Karatzas. Scene text visual question answering. In *ICCV*, pages 4291–4301, 2019. 9
- [9] Minwoo Byeon, Beomhee Park, Haecheon Kim, Sungjun Lee, Woonhyuk Baek, and Saehoon Kim. Coyo-700m: Image-text pair dataset. <https://github.com/kakaobrain/coyo-dataset>, 2022. 5, 9
- [10] Zheng Cai, Maosong Cao, Haojiong Chen, Kai Chen, Keyu Chen, Xin Chen, Xun Chen, Zehui Chen, Zhi Chen, Pei Chu, et al. Internlm2 technical report. *arXiv preprint arXiv:2403.17297*, 2024. 5
- [11] Jie Cao and Jing Xiao. An augmented benchmark dataset for geometric question answering through dual parallel text encoding. In *COLING*, pages 1511–1520, 2022. 9
- [12] Jimmy Carter. Textocr-gpt4v. <https://huggingface.co/datasets/jimmycarter/textocr-gpt4v>, 2024. 9
- [13] Shuaichen Chang, David Palzer, Jialin Li, Eric Fosler-Lussier, and Ningchuan Xiao. Mapqa: A dataset for question answering on choropleth maps. *arXiv preprint arXiv:2211.08545*, 2022. 9
- [14] Guiming Hardy Chen, Shunian Chen, Ruifei Zhang, Junying Chen, Xiangbo Wu, Zhiyi Zhang, Zhihong Chen, Jianquan Li, Xiang Wan, and Benyou Wang. Allava: Harnessing gpt4v-synthesized data for a lite vision-language model. *arXiv preprint arXiv:2402.11684*, 2024. 9
- [15] Jiaqi Chen, Tong Li, Jinghui Qin, Pan Lu, Liang Lin, Chongyu Chen, and Xiaodan Liang. Unigeo: Unifying geometry logical reasoning via reformulating mathematical expression. *arXiv preprint arXiv:2212.02746*, 2022. 9
- [16] Keqin Chen, Zhao Zhang, Weili Zeng, Richong Zhang, Feng Zhu, and Rui Zhao. Shikra: Unleashing multimodal llm’s referential dialogue magic. *arXiv preprint arXiv:2306.15195*, 2023. 9
- [17] Lin Chen, Xilin Wei, Jinsong Li, Xiaoyi Dong, Pan Zhang, Yuhang Zang, Zehui Chen, Haodong Duan, Bin Lin, Zhenyu Tang, et al. Sharegpt4video: Improving video understanding and generation with better captions. *arXiv preprint arXiv:2406.04325*, 2024. 9, 10
- [18] Zhe Chen, Weiyun Wang, Hao Tian, Shenglong Ye, Zhangwei Gao, Erfei Cui, Wenwen Tong, Kongzhi Hu, Jiapeng Luo, Zheng Ma, et al. How far are we to gpt-4v? closing the gap to commercial multimodal models with open-source suites. *arXiv preprint arXiv:2404.16821*, 2024. 1, 2, 3, 5, 10
- [19] Zhe Chen, Jiannan Wu, Wenhai Wang, Weijie Su, Guo Chen, Sen Xing, Muyan Zhong, Qinglong Zhang, Xizhou Zhu, Lewei Lu, et al. Internvl: Scaling up vision foundation models and aligning for generic visual-linguistic tasks. In *CVPR*, pages 24185–24198, 2024. 1, 2
- [20] Zesen Cheng, Sicong Leng, Hang Zhang, Yifei Xin, Xin Li, Guanzheng Chen, Yongxin Zhu, Wenqi Zhang, Ziyang Luo, Deli Zhao, et al. Videollama 2: Advancing spatial-temporal modeling and audio understanding in video-llms. *arXiv preprint arXiv:2406.07476*, 2024. 3, 6
- [21] Zewen Chi, Heyan Huang, Heng-Da Xu, Houjin Yu, Wanxuan Yin, and Xian-Ling Mao. Complicated table structure recognition. *arXiv preprint arXiv:1908.04729*, 2019. 9
- [22] Chee Kheng Chng, Yuliang Liu, Yipeng Sun, Chun Chet Ng, Canjie Luo, Zihan Ni, ChuanMing Fang, Shuaitao Zhang, Junyu Han, Errui Ding, et al. Icdar2019 robust reading challenge on arbitrary-shaped text-rrc-art. In *ICDAR*, pages 1571–1576. IEEE, 2019. 9
- [23] Christopher Clark and Matt Gardner. Simple and effective multi-paragraph reading comprehension. *arXiv preprint arXiv:1710.10723*, 2017. 9
- [24] Brian Davis, Bryan Morse, Scott Cohen, Brian Price, and Chris Tensmeyer. Deep visual template-free form parsing. In *ICDAR*, pages 134–141. IEEE, 2019. 9
- [25] Alexey Dosovitskiy, Lucas Beyer, Alexander Kolesnikov, Dirk Weissenborn, Xiaohua Zhai, Thomas Unterthiner, Mostafa Dehghani, Matthias Minderer, Georg Heigold, Sylvain Gelly, Jakob Uszkoreit, and Neil Houlsby. An image is worth 16x16 words: Transformers for image recognition at scale. In *ICLR*, 2021. 3, 5
- [26] Miquel Farré, Andi Marafioti, Lewis Tunstall, Leandro Von Werra, and Thomas Wolf. Finevideo. <https://huggingface.co/datasets/HuggingFaceFV/finevideo>, 2024. 9, 10
- [27] Jiajun Fei, Dian Li, Zhidong Deng, Zekun Wang, Gang Liu, and Hui Wang. Video-ccam: Enhancing video-language understanding with causal cross-attention masks for short and long videos. *arXiv preprint arXiv:2408.14023*, 2024. 3, 6
- [28] Chaoyou Fu, Peixian Chen, Yunhang Shen, Yulei Qin, Mengdan Zhang, Xu Lin, Jinrui Yang, Xiawu Zheng, Ke

- Li, Xing Sun, Yunsheng Wu, and Rongrong Ji. Mme: A comprehensive evaluation benchmark for multimodal large language models. *arXiv preprint arXiv:2306.13394*, 2023. 5
- [29] Chaoyou Fu, Yuhan Dai, Yongdong Luo, Lei Li, Shuhuai Ren, Renrui Zhang, Zihan Wang, Chenyu Zhou, Yunhang Shen, Mengdan Zhang, et al. Video-mme: The first-ever comprehensive evaluation benchmark of multi-modal llms in video analysis. *arXiv preprint arXiv:2405.21075*, 2024. 2, 5
- [30] Yash Goyal, Tejas Khot, Douglas Summers-Stay, Dhruv Batra, and Devi Parikh. Making the v in vqa matter: Elevating the role of image understanding in visual question answering. In *CVPR*, pages 6904–6913, 2017. 9
- [31] Jiayi Gu, Xiaojun Meng, Guansong Lu, Lu Hou, Niu Minzhe, Xiaodan Liang, Lewei Yao, Runhui Huang, Wei Zhang, Xin Jiang, et al. Wukong: A 100 million large-scale chinese cross-modal pre-training benchmark. *NeurIPS*, 35: 26418–26431, 2022. 9
- [32] He Guo, Xiameng Qin, Jiaming Liu, Junyu Han, Jingtuo Liu, and Errui Ding. Eaten: Entity-aware attention for single shot visual text extraction. In *ICDAR*, pages 254–259. IEEE, 2019. 9
- [33] Mengchao He, Yuliang Liu, Zhibo Yang, Sheng Zhang, Canjie Luo, Feiyu Gao, Qi Zheng, Yongpan Wang, Xin Zhang, and Lianwen Jin. Icp2018 contest on robust reading for multi-type web images. In *ICPR*, pages 7–12. IEEE, 2018. 9
- [34] Xuehai He, Yichen Zhang, Luntian Mou, Eric Xing, and Pengtao Xie. Pathvqa: 30000+ questions for medical visual question answering. *arXiv preprint arXiv:2003.10286*, 2020. 9
- [35] Dan Hendrycks and Kevin Gimpel. Gaussian error linear units (gelus). *arXiv preprint arXiv:1606.08415*, 2016. 4
- [36] Vlad Hosu, Hanhe Lin, Tamas Sziranyi, and Dietmar Saupe. Koniq-10k: An ecologically valid database for deep learning of blind image quality assessment. *IEEE TIP*, 29: 4041–4056, 2020. 9
- [37] Anwen Hu, Haiyang Xu, Jiabo Ye, Ming Yan, Liang Zhang, Bo Zhang, Chen Li, Ji Zhang, Qin Jin, Fei Huang, et al. mplug-docowl 1.5: Unified structure learning for ocr-free document understanding. *arXiv preprint arXiv:2403.12895*, 2024. 9
- [38] Xinyue Hu, L Gu, Q An, M Zhang, L Liu, K Kobayashi, T Harada, R Summers, and Y Zhu. Medical-diff-vqa: a large-scale medical dataset for difference visual question answering on chest x-ray images, 2023. 9
- [39] Qingqiu Huang, Yu Xiong, Anyi Rao, Jiase Wang, and Dahua Lin. Movienet: A holistic dataset for movie understanding. In *ECCV*, pages 709–727. Springer, 2020. 9
- [40] Zheng Huang, Kai Chen, Jianhua He, Xiang Bai, Dimosthenis Karatzas, Shijian Lu, and CV Jawahar. Icdar2019 competition on scanned receipt ocr and information extraction. In *ICDAR*, pages 1516–1520. IEEE, 2019. 9
- [41] Drew A Hudson and Christopher D Manning. Gqa: A new dataset for real-world visual reasoning and compositional question answering. In *CVPR*, pages 6700–6709, 2019. 9
- [42] Baoxiong Jia, Ting Lei, Song-Chun Zhu, and Siyuan Huang. Egotaskqa: Understanding human tasks in egocentric videos. *NeurIPS*, 35:3343–3360, 2022. 9, 10
- [43] Yiren Jian, Tingkai Liu, Yunzhe Tao, Chunhui Zhang, Soroush Vosoughi, and Hongxia Yang. Expedited training of visual conditioned language generation via redundancy reduction. In *ACL*, pages 300–314, 2024. 3
- [44] Justin Johnson, Bharath Hariharan, Laurens Van Der Maaten, Li Fei-Fei, C Lawrence Zitnick, and Ross Girshick. Clevr: A diagnostic dataset for compositional language and elementary visual reasoning. In *CVPR*, pages 2901–2910, 2017. 9
- [45] Xuan Ju, Yiming Gao, Zhaoyang Zhang, Ziyang Yuan, Xintao Wang, Ailing Zeng, Yu Xiong, Qiang Xu, and Ying Shan. Miradata: A large-scale video dataset with long durations and structured captions. *arXiv preprint arXiv:2407.06358*, 2024. 9, 10
- [46] Kushal Kafle, Brian Price, Scott Cohen, and Christopher Kanan. Dvqa: Understanding data visualizations via question answering. In *CVPR*, pages 5648–5656, 2018. 9
- [47] Samira Ebrahimi Kahou, Vincent Michalski, Adam Atkinson, Ákos Kádár, Adam Trischler, and Yoshua Bengio. Figureqa: An annotated figure dataset for visual reasoning. *arXiv preprint arXiv:1710.07300*, 2017. 9
- [48] Shankar Kantharaj, Rixie Tiffany Ko Leong, Xiang Lin, Ahmed Masry, Megh Thakkar, Enamul Hoque, and Shafiq Joty. Chart-to-text: A large-scale benchmark for chart summarization. *arXiv preprint arXiv:2203.06486*, 2022. 9
- [49] Sahar Kazemzadeh, Vicente Ordonez, Mark Matten, and Tamara Berg. Referitgame: Referring to objects in photographs of natural scenes. In *EMNLP*, pages 787–798, 2014. 9
- [50] Aniruddha Kembhavi, Mike Salvato, Eric Kolve, Minjoon Seo, Hannaneh Hajishirzi, and Ali Farhadi. A diagram is worth a dozen images. In *ECCV*, pages 235–251, 2016. 5, 9
- [51] Aniruddha Kembhavi, Minjoon Seo, Dustin Schwenk, Jonghyun Choi, Ali Farhadi, and Hannaneh Hajishirzi. Are you smarter than a sixth grader? textbook question answering for multimodal machine comprehension. In *CVPR*, pages 4999–5007, 2017. 9
- [52] Diederik P Kingma. Adam: A method for stochastic optimization. *arXiv preprint arXiv:1412.6980*, 2014. 5
- [53] Jianfeng Kuang, Wei Hua, Dingkan Liang, Mingkun Yang, Deqiang Jiang, Bo Ren, and Xiang Bai. Visual information extraction in the wild: practical dataset and end-to-end solution. In *ICDAR*, pages 36–53. Springer, 2023. 9
- [54] LAION. Laion-gpt4v dataset. <https://huggingface.co/datasets/laion/gpt4v-dataset>, 2023. 9
- [55] Jason J Lau, Soumya Gayen, Asma Ben Abacha, and Dina Demner-Fushman. A dataset of clinically generated visual questions and answers about radiology images. *Scientific data*, 5(1):1–10, 2018. 9
- [56] Jie Lei, Licheng Yu, Mohit Bansal, and Tamara L Berg. Tvqa: Localized, compositional video question answering. *arXiv preprint arXiv:1809.01696*, 2018. 9, 10

- [57] Paul Lerner, Olivier Ferret, Camille Guinaudeau, Hervé Le Borgne, Romaric Besançon, José G Moreno, and Jesús Lovón Melgarejo. Viquae, a dataset for knowledge-based visual question answering about named entities. In *SIGIR*, pages 3108–3120, 2022. 9
- [58] Bohao Li, Rui Wang, Guangzhi Wang, Yuying Ge, Yixiao Ge, and Ying Shan. Seed-bench: Benchmarking multimodal llms with generative comprehension. *arXiv preprint arXiv:2307.16125*, 2023. 5
- [59] Bo Li, Yuanhan Zhang, Dong Guo, Renrui Zhang, Feng Li, Hao Zhang, Kaichen Zhang, Yanwei Li, Ziwei Liu, and Chunyuan Li. Llava-onevision: Easy visual task transfer. *arXiv preprint arXiv:2408.03326*, 2024. 1, 2, 3, 5, 6, 7, 10, 11
- [60] Feng Li, Renrui Zhang, Hao Zhang, Yuanhan Zhang, Bo Li, Wei Li, Zejun Ma, and Chunyuan Li. Llava-next-interleave: Tackling multi-image, video, and 3d in large multimodal models. *arXiv preprint arXiv:2407.07895*, 2024. 2
- [61] Junnan Li, Dongxu Li, Silvio Savarese, and Steven Hoi. Blip-2: Bootstrapping language-image pre-training with frozen image encoders and large language models. In *ICML*, pages 19730–19742, 2023. 3
- [62] Junxian Li, Di Zhang, Xunzhi Wang, Zeying Hao, Jingdi Lei, Qian Tan, Cai Zhou, Wei Liu, Yaotian Yang, Xinrui Xiong, et al. Chemvlm: Exploring the power of multimodal large language models in chemistry area. *arXiv preprint arXiv:2408.07246*, 2024. 9
- [63] KunChang Li, Yinan He, Yi Wang, Yizhuo Li, Wenhai Wang, Ping Luo, Yali Wang, Limin Wang, and Yu Qiao. Videochat: Chat-centric video understanding. *arXiv preprint arXiv:2305.06355*, 2023. 3
- [64] Kunchang Li, Yali Wang, Yinan He, Yizhuo Li, Yi Wang, Yi Liu, Zun Wang, Jilan Xu, Guo Chen, Ping Luo, et al. Mvbench: A comprehensive multi-modal video understanding benchmark. In *CVPR*, pages 22195–22206, 2024. 2, 3, 5, 6, 9, 10
- [65] Yanwei Li, Chengyao Wang, and Jiaya Jia. Llama-vid: An image is worth 2 tokens in large language models. In *ECCV*, pages 323–340, 2025. 3
- [66] Zhuowan Li, Xingrui Wang, Elias Stengel-Eskin, Adam Kortylewski, Wufei Ma, Benjamin Van Durme, and Alan L Yuille. Super-clevr: A virtual benchmark to diagnose domain robustness in visual reasoning. In *CVPR*, pages 14963–14973, 2023. 9
- [67] Tsung-Yi Lin, Michael Maire, Serge Belongie, James Hays, Pietro Perona, Deva Ramanan, Piotr Dollár, and C Lawrence Zitnick. Microsoft coco: Common objects in context. In *ECCV*, pages 740–755. Springer, 2014. 9
- [68] Bo Liu, Li-Ming Zhan, Li Xu, Lin Ma, Yan Yang, and Xiao-Ming Wu. Slake: A semantically-labeled knowledge-enhanced dataset for medical visual question answering. In *ISBI*, pages 1650–1654. IEEE, 2021. 9
- [69] Cheng-Lin Liu, Fei Yin, Da-Han Wang, and Qiu-Feng Wang. Casia online and offline chinese handwriting databases. In *ICDAR*, pages 37–41. IEEE, 2011. 9
- [70] Fangyu Liu, Guy Emerson, and Nigel Collier. Visual spatial reasoning. *Transactions of the Association for Computational Linguistics*, 11:635–651, 2023. 9
- [71] Fuxiao Liu, Kevin Lin, Linjie Li, Jianfeng Wang, Yaser Yacoob, and Lijuan Wang. Mitigating hallucination in large multi-modal models via robust instruction tuning. In *ICLR*, 2023. 9
- [72] Fuxiao Liu, Xiaoyang Wang, Wenlin Yao, Jianshu Chen, Kaiqiang Song, Sangwoo Cho, Yaser Yacoob, and Dong Yu. Mmc: Advancing multimodal chart understanding with large-scale instruction tuning. *arXiv preprint arXiv:2311.10774*, 2023. 9
- [73] Haotian Liu, Chunyuan Li, Yuheng Li, and Yong Jae Lee. Improved baselines with visual instruction tuning. In *CVPR*, pages 26296–26306, 2024. 1, 2
- [74] Haotian Liu, Chunyuan Li, Qingyang Wu, and Yong Jae Lee. Visual instruction tuning. *NeurIPS*, 36, 2024. 1, 2, 5, 10
- [75] Jiajun Liu, Yibing Wang, Hanghang Ma, Xiaoping Wu, Xiaoqi Ma, Xiaoming Wei, Jianbin Jiao, Enhua Wu, and Jie Hu. Kangaroo: A powerful video-language model supporting long-context video input. *arXiv preprint arXiv:2408.15542*, 2024. 3, 6
- [76] Ruyang Liu, Chen Li, Haoran Tang, Yixiao Ge, Ying Shan, and Ge Li. St-llm: Large language models are effective temporal learners. In *ECCV*, pages 1–18, 2025. 3
- [77] Yuliang Liu, Zhang Li, Biao Yang, Chunyuan Li, Xucheng Yin, Cheng-lin Liu, Lianwen Jin, and Xiang Bai. On the hidden mystery of ocr in large multimodal models. *arXiv preprint arXiv:2305.07895*, 2023. 5
- [78] Yuan Liu, Haodong Duan, Yuanhan Zhang, Bo Li, Songyang Zhang, Wangbo Zhao, Yike Yuan, Jiaqi Wang, Conghui He, Ziwei Liu, et al. Mmbench: Is your multimodal model an all-around player? In *ECCV*, pages 216–233, 2025. 5
- [79] Ze Liu, Jia Ning, Yue Cao, Yixuan Wei, Zheng Zhang, Stephen Lin, and Han Hu. Video swin transformer. In *CVPR*, pages 3202–3211, 2022. 3
- [80] Ziyu Liu, Tao Chu, Yuhang Zang, Xilin Wei, Xiaoyi Dong, Pan Zhang, Zijian Liang, Yuanjun Xiong, Yu Qiao, Dahua Lin, et al. Mmdu: A multi-turn multi-image dialog understanding benchmark and instruction-tuning dataset for lvlms. *arXiv preprint arXiv:2406.11833*, 2024. 9
- [81] Zuyan Liu, Yuhao Dong, Ziwei Liu, Winston Hu, Jiwen Lu, and Yongming Rao. Oryx mllm: On-demand spatial-temporal understanding at arbitrary resolution. *arXiv preprint arXiv:2409.12961*, 2024. 3, 6, 7
- [82] Pan Lu, Ran Gong, Shibiao Jiang, Liang Qiu, Siyuan Huang, Xiaodan Liang, and Song-Chun Zhu. Inter-gps: Interpretable geometry problem solving with formal language and symbolic reasoning. *arXiv preprint arXiv:2105.04165*, 2021. 9
- [83] Pan Lu, Swaroop Mishra, Tanglin Xia, Liang Qiu, Kai-Wei Chang, Song-Chun Zhu, Oyvind Tafjord, Peter Clark, and Ashwin Kalyan. Learn to explain: Multimodal reasoning via thought chains for science question answering. *NeurIPS*, 35:2507–2521, 2022. 5, 9
- [84] Pan Lu, Liang Qiu, Kai-Wei Chang, Ying Nian Wu, Song-Chun Zhu, Tanmay Rajpurohit, Peter Clark, and Ashwin Kalyan. Dynamic prompt learning via policy gradient for

- semi-structured mathematical reasoning. *arXiv preprint arXiv:2209.14610*, 2022. 9
- [85] Muhammad Maaz, Hanoona Rasheed, Salman Khan, and Fahad Khan. Videogpt+: Integrating image and video encoders for enhanced video understanding. *arXiv preprint arXiv:2406.09418*, 2024. 9, 10
- [86] Muhammad Maaz, Hanoona Rasheed, Salman Khan, and Fahad Shahbaz Khan. Video-chatgpt: Towards detailed video understanding via large vision and language models. In *ACL*, pages 12585–12602, 2024. 3
- [87] Karttikeya Mangalam, Raiymbek Akshulakov, and Jitendra Malik. Egoschema: A diagnostic benchmark for very long-form video language understanding. *NeurIPS*, 36:46212–46244, 2023. 5
- [88] Hui Mao, Ming Cheung, and James She. Deepart: Learning joint representations of visual arts. In *ACM MM*, pages 1183–1191, 2017. 9
- [89] Kenneth Marino, Mohammad Rastegari, Ali Farhadi, and Roozbeh Mottaghi. Ok-vqa: A visual question answering benchmark requiring external knowledge. In *CVPR*, pages 3195–3204, 2019. 9
- [90] U-V Marti and Horst Bunke. The iam-database: an english sentence database for offline handwriting recognition. *International journal on document analysis and recognition*, 5:39–46, 2002. 9
- [91] Ahmed Masry, Xuan Long Do, Jia Qing Tan, Shafiq Joty, and Enamul Hoque. Chartqa: A benchmark for question answering about charts with visual and logical reasoning. In *ACL*, pages 2263–2279, 2022. 5, 9
- [92] Ahmed Masry, Parsa Kavehzadeh, Xuan Long Do, Enamul Hoque, and Shafiq Joty. Unichart: A universal vision-language pretrained model for chart comprehension and reasoning. *arXiv preprint arXiv:2305.14761*, 2023. 9
- [93] Minesh Mathew, Dimosthenis Karatzas, and CV Jawahar. Docvqa: A dataset for vqa on document images. In *WACV*, pages 2200–2209, 2021. 2, 5
- [94] Minesh Mathew, Viraj Bagal, Rubèn Tito, Dimosthenis Karatzas, Ernest Valveny, and CV Jawahar. Infographicvqa. In *WACV*, pages 1697–1706, 2022. 2, 5, 9
- [95] Nitesh Methani, Pritha Ganguly, Mitesh M Khapra, and Pratyush Kumar. Plotqa: Reasoning over scientific plots. In *WACV*, pages 1527–1536, 2020. 9
- [96] Kepan Nan, Rui Xie, Penghao Zhou, Tiehan Fan, Zhenheng Yang, Zhijie Chen, Xiang Li, Jian Yang, and Ying Tai. Openvid-1m: A large-scale high-quality dataset for text-to-video generation. *arXiv preprint arXiv:2407.02371*, 2024. 9
- [97] OpenAI. Gpt-4v(ision) system card, 2023. 1, 2, 6, 7
- [98] OpenAI. Hello gpt-4o, 2024. 1, 2, 6, 7
- [99] Viorica Patraucean, Lucas Smaira, Ankush Gupta, Adria Recasens, Larisa Markeeva, Dylan Banarse, Skanda Koppala, Mateusz Malinowski, Yi Yang, Carl Doersch, et al. Perception test: A diagnostic benchmark for multimodal video models. *NeurIPS*, 36, 2024. 5, 9
- [100] William Peebles and Saining Xie. Scalable diffusion models with transformers. In *ICCV*, pages 4195–4205, 2023. 4, 5
- [101] Zhiliang Peng, Wenhui Wang, Li Dong, Yaru Hao, Shaohan Huang, Shuming Ma, and Furu Wei. Kosmos-2: Grounding multimodal large language models to the world. *arXiv preprint arXiv:2306.14824*, 2023. 9
- [102] Shuhuai Ren, Sishuo Chen, Shicheng Li, Xu Sun, and Lu Hou. Testa: Temporal-spatial token aggregation for long-form video-language understanding. In *EMNLP*, pages 932–947, 2023. 3
- [103] Anna Rohrbach, Marcus Rohrbach, Niket Tandon, and Bernt Schiele. A dataset for movie description. In *CVPR*, pages 3202–3212, 2015. 9, 10
- [104] Michael S Ryoo, Honglu Zhou, Shrikant Kendre, Can Qin, Le Xue, Manli Shu, Silvio Savarese, Ran Xu, Caiming Xiong, and Juan Carlos Niebles. xgen-mm-vid (blip-3-video): You only need 32 tokens to represent a video even in vlms. *arXiv preprint arXiv:2410.16267*, 2024. 3, 6
- [105] Christoph Schuhmann, Romain Beaumont, Richard Vencu, Cade Gordon, Ross Wightman, Mehdi Cherti, Theo Coombes, Aarush Katta, Clayton Mullis, Mitchell Wortsman, et al. Laion-5b: An open large-scale dataset for training next generation image-text models. *NeurIPS*, 35: 25278–25294, 2022. 5, 9
- [106] Christoph Schuhmann, Andreas Köpf, Richard Vencu, Theo Coombes, and Romain Beaumont. Laion coco: 600m synthetic captions from laion2b-en. <https://laion.ai/blog/laion-coco/>, 2022. 9
- [107] Minjoon Seo, Hannaneh Hajishirzi, Ali Farhadi, Oren Etzioni, and Clint Malcol. Solving geometry problems: Combining text and diagram interpretation. In *EMNLP*, pages 1466–1476, 2015. 9
- [108] Sanket Shah, Anand Mishra, Naganand Yadati, and Partha Pratim Talukdar. Kvqa: Knowledge-aware visual question answering. In *AAAI*, pages 8876–8884, 2019. 9
- [109] Amir Shahroudy, Jun Liu, Tian-Tsong Ng, and Gang Wang. Ntu rgb+d: A large scale dataset for 3d human activity analysis. In *CVPR*, pages 1010–1019, 2016. 9, 10
- [110] Shuai Shao, Zeming Li, Tianyuan Zhang, Chao Peng, Gang Yu, Xiangyu Zhang, Jing Li, and Jian Sun. Objects365: A large-scale, high-quality dataset for object detection. In *ICCV*, pages 8430–8439, 2019. 9
- [111] Xiaoqian Shen, Yunyang Xiong, Changsheng Zhao, Lemeng Wu, Jun Chen, Chenchen Zhu, Zechun Liu, Fanyi Xiao, Balakrishnan Varadarajan, Florian Bordes, et al. Longvu: Spatiotemporal adaptive compression for long video-language understanding. *arXiv preprint arXiv:2410.17434*, 2024. 3, 6
- [112] Wenzhe Shi, Jose Caballero, Ferenc Huszár, Johannes Totz, Andrew P Aitken, Rob Bishop, Daniel Rueckert, and Zehan Wang. Real-time single image and video super-resolution using an efficient sub-pixel convolutional neural network. In *CVPR*, pages 1874–1883, 2016. 2, 5
- [113] Amanpreet Singh, Vivek Natarajan, Meet Shah, Yu Jiang, Xinlei Chen, Dhruv Batra, Devi Parikh, and Marcus Rohrbach. Towards vqa models that can read. In *CVPR*, pages 8317–8326, 2019. 5, 9
- [114] Amanpreet Singh, Guan Pang, Mandy Toh, Jing Huang, Wojciech Galuba, and Tal Hassner. Textocr: Towards large-

- scale end-to-end reasoning for arbitrary-shaped scene text. In *CVPR*, pages 8802–8812, 2021. 9
- [115] Yipeng Sun, Zihan Ni, Chee-Kheng Chng, Yuliang Liu, Canjie Luo, Chun Chet Ng, Junyu Han, Errui Ding, Jingtuo Liu, Dimosthenis Karatzas, et al. Icdar 2019 competition on large-scale street view text with partial labeling-rrc-lsvt. In *ICDAR*, pages 1557–1562. IEEE, 2019. 9
- [116] Gemini Team, Rohan Anil, Sebastian Borgeaud, Yonghui Wu, Jean-Baptiste Alayrac, Jiahui Yu, Radu Soricut, Johan Schalkwyk, Andrew M Dai, Anja Hauth, et al. Gemini: A family of highly capable multimodal models. *arXiv:2312.11805*, 2023. 1, 2, 6, 7
- [117] OpenGVLab Team. Internvl2: Better than the best—expanding performance boundaries of open-source multimodal models with the progressive scaling strategy, 2024. 1, 2, 3, 5, 6, 7, 9, 10, 11
- [118] A Vaswani. Attention is all you need. *NeurIPS*, 2017. 4
- [119] Andreas Veit, Tomas Matera, Lukas Neumann, Jiri Matas, and Serge Belongie. Coco-text: Dataset and benchmark for text detection and recognition in natural images. *arXiv preprint arXiv:1601.07140*, 2016. 9
- [120] Jiaqi Wang, Pan Zhang, Tao Chu, Yuhang Cao, Yujie Zhou, Tong Wu, Bin Wang, Conghui He, and Dahua Lin. V3det: Vast vocabulary visual detection dataset. In *ICCV*, pages 19844–19854, 2023. 9
- [121] Jiawei Wang, Liping Yuan, Yuchen Zhang, and Hao-miao Sun. Tarsier: Recipes for training and evaluating large video description models. *arXiv preprint arXiv:2407.00634*, 2024. 6
- [122] Peng Wang, Shuai Bai, Sinan Tan, Shijie Wang, Zhihao Fan, Jinze Bai, Keqin Chen, Xuejing Liu, Jialin Wang, Wenbin Ge, et al. Qwen2-vl: Enhancing vision-language model’s perception of the world at any resolution. *arXiv preprint arXiv:2409.12191*, 2024. 1, 2, 3, 5, 6, 7, 10, 11
- [123] Weiyun Wang, Min Shi, Qingyun Li, Wenhai Wang, Zhenhang Huang, Linjie Xing, Zhe Chen, Hao Li, Xizhou Zhu, Zhiguo Cao, et al. The all-seeing project: Towards panoptic visual recognition and understanding of the open world. *arXiv preprint arXiv:2308.01907*, 2023. 9
- [124] Xinyu Wang, Yuliang Liu, Chunhua Shen, Chun Chet Ng, Canjie Luo, Lianwen Jin, Chee Seng Chan, Anton van den Hengel, and Liangwei Wang. On the general value of evidence, and bilingual scene-text visual question answering. In *CVPR*, pages 10126–10135, 2020. 9
- [125] Xidong Wang, Dingjie Song, Shunian Chen, Chen Zhang, and Benyou Wang. Longllava: Scaling multi-modal llms to 1000 images efficiently via hybrid architecture. *arXiv preprint arXiv:2409.02889*, 2024. 3
- [126] Xiyao Wang, Yuhang Zhou, Xiaoyu Liu, Hongjin Lu, Yuancheng Xu, Feihong He, Jaehong Yoon, Taixi Lu, Gedas Bertasius, Mohit Bansal, et al. Mementos: A comprehensive benchmark for multimodal large language model reasoning over image sequences. *arXiv preprint arXiv:2401.10529*, 2024. 9, 10
- [127] Yi Wang, Yanan He, Yizhuo Li, Kunchang Li, Jiashuo Yu, Xin Ma, Xinhao Li, Guo Chen, Xinyuan Chen, Yaohui Wang, et al. Internvid: A large-scale video-text dataset for multimodal understanding and generation. *arXiv preprint arXiv:2307.06942*, 2023. 5, 9
- [128] Yi Wang, Kunchang Li, Xinhao Li, Jiashuo Yu, Yanan He, Guo Chen, Baoqi Pei, Rongkun Zheng, Jilan Xu, Zun Wang, et al. Internvideo2: Scaling video foundation models for multimodal video understanding. *arXiv preprint arXiv:2403.15377*, 2024. 6
- [129] Bo Wu, Shoubin Yu, Zhenfang Chen, Joshua B Tenenbaum, and Chuang Gan. Star: A benchmark for situated reasoning in real-world videos. *arXiv preprint arXiv:2405.09711*, 2024. 9, 10
- [130] Chaoyi Wu. Pmc-casereport. <https://huggingface.co/datasets/chaoyi-wu/PMC-CaseReport>, 2023. 9
- [131] Haoning Wu, Dongxu Li, Bei Chen, and Junnan Li. Longvideobench: A benchmark for long-context interleaved video-language understanding. *arXiv preprint arXiv:2407.15754*, 2024. 5
- [132] Weijia Wu, Yuzhong Zhao, Zhuang Li, Jiahong Li, Hong Zhou, Mike Zheng Shou, and Xiang Bai. A large cross-modal video retrieval dataset with reading comprehension. *Pattern Recognition*, 157:110818, 2025. 9
- [133] Junbin Xiao, Xindi Shang, Angela Yao, and Tat-Seng Chua. Next-qa: Next phase of question-answering to explaining temporal actions. In *CVPR*, pages 9777–9786, 2021. 5
- [134] Lin Xu, Yilin Zhao, Daquan Zhou, Zhijie Lin, See Kiong Ng, and Jiashi Feng. Pillava: Parameter-free llava extension from images to videos for video dense captioning. *arXiv preprint arXiv:2404.16994*, 2024. 3, 6
- [135] Dongjie Yang, Suyuan Huang, Chengqiang Lu, Xiaodong Han, Haoxin Zhang, Yan Gao, Yao Hu, and Hai Zhao. Vript: A video is worth thousands of words. *arXiv preprint arXiv:2406.06040*, 2024. 5, 9, 10
- [136] Yuan Yao, Tianyu Yu, Ao Zhang, Chongyi Wang, Junbo Cui, Hongji Zhu, Tianchi Cai, Haoyu Li, Weilin Zhao, Zhihui He, et al. Minicpm-v: A gpt-4v level mllm on your phone. *arXiv preprint arXiv:2408.01800*, 2024. 3
- [137] Kexin Yi, Chuang Gan, Yunzhu Li, Pushmeet Kohli, Jiajun Wu, Antonio Torralba, and Joshua B Tenenbaum. Clevrer: Collision events for video representation and reasoning. *arXiv preprint arXiv:1910.01442*, 2019. 9, 10
- [138] Longhui Yu, Weisen Jiang, Han Shi, Jincheng Yu, Zhengying Liu, Yu Zhang, James T Kwok, Zhenguo Li, Adrian Weller, and Weiyang Liu. Metamath: Bootstrap your own mathematical questions for large language models. *arXiv preprint arXiv:2309.12284*, 2023. 9
- [139] Zhou Yu, Dejing Xu, Jun Yu, Ting Yu, Zhou Zhao, Yueting Zhuang, and Dacheng Tao. Activitynet-qa: A dataset for understanding complex web videos via question answering. In *AAAI*, pages 9127–9134, 2019. 5
- [140] Tai-Ling Yuan, Zhe Zhu, Kun Xu, Cheng-Jun Li, Tai-Jiang Mu, and Shi-Min Hu. A large chinese text dataset in the wild. *J. Comput. Sci. Tech.*, 34(3):509–521, 2019. 9
- [141] Ye Yuan, Xiao Liu, Wondimu Dikubab, Hui Liu, Zhilong Ji, Zhongqin Wu, and Xiang Bai. Syntax-aware network for handwritten mathematical expression recognition. *arXiv preprint arXiv:2203.01601*, 2022. 9

- [142] Xiang Yue, Yuansheng Ni, Kai Zhang, Tianyu Zheng, Ruoqi Liu, Ge Zhang, Samuel Stevens, Dongfu Jiang, Weiming Ren, Yuxuan Sun, et al. Mmmu: A massive multi-discipline multimodal understanding and reasoning benchmark for expert agi. In *CVPR*, pages 9556–9567, 2024. [5](#)
- [143] Abhay Zala, Jaemin Cho, Satwik Kottur, Xilun Chen, Barlas Öğuz, Yashar Mehdad, and Mohit Bansal. Hierarchical video-moment retrieval and step-captioning. In *CVPR*, 2023. [9](#), [10](#)
- [144] Hang Zhang, Xin Li, and Lidong Bing. Video-llama: An instruction-tuned audio-visual language model for video understanding. In *EMNLP: System Demonstrations*, pages 543–553, 2023. [3](#)
- [145] Pan Zhang, Xiaoyi Dong, Yuhang Zang, Yuhang Cao, Rui Qian, Lin Chen, Qipeng Guo, Haodong Duan, Bin Wang, Linke Ouyang, et al. Internlm-xcomposer-2.5: A versatile large vision language model supporting long-contextual input and output. *arXiv preprint arXiv:2407.03320*, 2024. [2](#), [6](#), [7](#)
- [146] Peiyuan Zhang, Kaichen Zhang, Bo Li, Guangtao Zeng, Jingkang Yang, Yuanhan Zhang, Ziyue Wang, Haoran Tan, Chunyuan Li, and Ziwei Liu. Long context transfer from language to vision. *arXiv preprint arXiv:2406.16852*, 2024. [3](#), [6](#), [7](#)
- [147] Rui Zhang, Yongsheng Zhou, Qianyi Jiang, Qi Song, Nan Li, Kai Zhou, Lei Wang, Dong Wang, Minghui Liao, Mingkun Yang, et al. Icdar 2019 robust reading challenge on reading chinese text on signboard. In *ICDAR*, pages 1577–1581. IEEE, 2019. [9](#)
- [148] Ruohong Zhang, Liangke Gui, Zhiqing Sun, Yihao Feng, Keyang Xu, Yuanhan Zhang, Di Fu, Chunyuan Li, Alexander Hauptmann, Yonatan Bisk, et al. Direct preference optimization of video large multimodal models from language model reward. *arXiv preprint arXiv:2404.01258*, 2024. [3](#)
- [149] Xiaoman Zhang, Chaoyi Wu, Ziheng Zhao, Weixiong Lin, Ya Zhang, Yanfeng Wang, and Weidi Xie. Pmc-vqa: Visual instruction tuning for medical visual question answering. *arXiv preprint arXiv:2305.10415*, 2023. [9](#)
- [150] Yanzhe Zhang, Ruiyi Zhang, Jiuxiang Gu, Yufan Zhou, Nedim Lipka, Diyi Yang, and Tong Sun. Llavav: Enhanced visual instruction tuning for text-rich image understanding. *arXiv preprint arXiv:2306.17107*, 2023. [9](#)
- [151] Yuanhan Zhang, Jinming Wu, Wei Li, Bo Li, Zejun Ma, Ziwei Liu, and Chunyuan Li. Video instruction tuning with synthetic data. *arXiv preprint arXiv:2410.02713*, 2024. [5](#), [6](#), [9](#), [10](#)
- [152] Xinyi Zheng, Douglas Burdick, Lucian Popa, Xu Zhong, and Nancy Xin Ru Wang. Global table extractor (gte): A framework for joint table identification and cell structure recognition using visual context. In *WACV*, pages 697–706, 2021. [9](#)
- [153] Junjie Zhou, Yan Shu, Bo Zhao, Boya Wu, Shitao Xiao, Xi Yang, Yongping Xiong, Bo Zhang, Tiejun Huang, and Zheng Liu. Mlvu: A comprehensive benchmark for multi-task long video understanding. *arXiv preprint arXiv:2406.04264*, 2024. [2](#), [5](#)